

# Solution of the Skyrme-Hartree-Fock-Bogolyubov equations in the Cartesian deformed harmonic-oscillator basis.

(VII) HFODD (v2.49t): a new version of the program.

N. Schunck,<sup>a,b,c1</sup> J. Dobaczewski,<sup>d,e</sup> J. McDonnell,<sup>b,c</sup> W. Satuła,<sup>d</sup> J.A. Sheikh,<sup>b,c</sup>  
A. Staszczak,<sup>b,c,f</sup> M. Stoitsov,<sup>b,c</sup> P. Toivanen<sup>e</sup>

<sup>a</sup>*Physics Division, Lawrence Livermore National Laboratory Livermore, CA 94551, USA*

<sup>b</sup>*Department of Physics and Astronomy, University of Tennessee, Knoxville, TN 37996, USA*

<sup>c</sup>*Oak Ridge National Laboratory, P.O. Box 2008, Oak Ridge, TN 37831, USA*

<sup>d</sup>*Institute of Theoretical Physics, Faculty of Physics, University of Warsaw,  
ul. Hoża 69, PL-00681 Warsaw, Poland*

<sup>e</sup>*Department of Physics, P.O. Box 35 (YFL), FI-40014 University of Jyväskylä, Finland*

<sup>f</sup>*Department of Theoretical Physics, Maria Curie-Skłodowska University,  
pl. M. Curie-Skłodowskiej 1, 20-031 Lublin, Poland*

---

## Abstract

We describe the new version (v2.49t) of the code HFODD which solves the nuclear Skyrme Hartree-Fock (HF) or Skyrme Hartree-Fock-Bogolyubov (HFB) problem by using the Cartesian deformed harmonic-oscillator basis. In the new version, we have implemented the following physics features: (i) the isospin mixing and projection, (ii) the finite temperature formalism for the HFB and HF+BCS methods, (iii) the Lipkin translational energy correction method, (iv) the calculation of the shell correction. A number of specific numerical methods have also been implemented in order to deal with large-scale multi-constraint calculations and hardware limitations: (i) the two-basis method for the HFB method, (ii) the Augmented Lagrangian Method (ALM) for multi-constraint calculations, (iii) the linear constraint method based on the approximation of the RPA matrix for multi-constraint calculations, (iv) an interface with the axial and parity-conserving Skyrme-HFB code HFBTHO, (v) the mixing of the HF or HFB matrix elements instead of the HF fields. Special care has been paid to using the code on massively parallel leadership class computers. For this purpose, the following features are now available with this version: (i) the Message Passing Interface (MPI) framework (ii) scalable input data routines (iii) multi-threading via OpenMP pragmas (iv) parallel diagonalization of the HFB matrix in the simplex breaking case using the ScaLAPACK library. Finally, several little significant errors of the previous published version were corrected.

---

PACS numbers: 07.05.T, 21.60.-n, 21.60.Jz

## NEW VERSION PROGRAM SUMMARY

*Title of the program:* HFODD (v2.49t)

---

<sup>1</sup>E-mail: schunck1@llnl.gov

*Catalogue number:* ....

*Program obtainable from:* CPC Program Library, Queen's University of Belfast, N. Ireland (see application form in this issue)

*Reference in CPC for earlier version of program:* J. Dobaczewski, W. Satuła, B.G. Carlsson, J. Engel, P. Olbratowski, P. Powalowski, M. Sadziak, J. Sarich, N. Schunck, A. Staszczak, M. Stoitsov, M. Zalewski, H. Zduńczuk, *Comput. Phys. Commun.* **180** (2009) 2361 (v2.40h).

*Catalogue number of previous version:* ADFL\_v2\_1

*Licensing provisions:* GPL v3

*Does the new version supersede the previous one:* yes

*Computers on which the program has been tested:* Intel Pentium-III, Intel Xeon, AMD-Athlon, AMD-Opteron, Cray XT4, Cray XT5

*Operating systems:* UNIX, LINUX, Windows<sup>xp</sup>

*Programming language used:* FORTRAN-90

*Memory required to execute with typical data:* 10 Mwords

*No. of bits in a word:* The code is written in single-precision for the use on a 64-bit processor. The compiler option `-r8` or `+autodblpad` (or equivalent) has to be used to promote all real and complex single-precision floating-point items to double precision when the code is used on a 32-bit machine.

*Has the code been vectorised?:* Yes

*Has the code been parallelized?:* Yes

*No. of lines in distributed program:* 104 666 (of which 47 059 are comments and separators)

*Keywords:* Hartree-Fock; Hartree-Fock-Bogolyubov; Skyrme interaction; Self-consistent mean field; Nuclear many-body problem; Superdeformation; Quadrupole deformation; Octupole deformation; Pairing; Nuclear radii; Single-particle spectra; Nuclear rotation; High-spin states; Moments of inertia; Level crossings; Harmonic oscillator; Coulomb field; Pairing; Point symmetries; Yukawa interaction; Angular-momentum projection; Generator Coordinate Method; Schiff moments; Isospin mixing; Isospin projection, Finite temperature; Shell correction; Lipkin method; Multi-threading; Hybrid programming model; High-performance computing.

*Nature of physical problem*

The nuclear mean field and an analysis of its symmetries in realistic cases are the main ingredients of a description of nuclear states. Within the Local Density Approximation, or for a zero-range velocity-dependent Skyrme interaction, the nuclear mean field is local and velocity dependent. The locality allows for an effective and fast solution of the self-consistent Hartree-Fock

equations, even for heavy nuclei, and for various nucleonic ( $n$ -particle  $n$ -hole) configurations, deformations, excitation energies, or angular momenta. Similarly, Local Density Approximation in the particle-particle channel, which is equivalent to using a zero-range interaction, allows for a simple implementation of pairing effects within the Hartree-Fock-Bogolyubov method.

#### *Method of solution*

The program uses the Cartesian harmonic oscillator basis to expand single-particle or single-quasiparticle wave functions of neutrons and protons interacting by means of the Skyrme effective interaction and zero-range pairing interaction. The expansion coefficients are determined by the iterative diagonalization of the mean-field Hamiltonians or Routhians which depend nonlinearly on the local neutron and proton densities. Suitable constraints are used to obtain states corresponding to a given configuration, deformation or angular momentum. The method of solution has been presented in: J. Dobaczewski and J. Dudek, *Comput. Phys. Commun.* **102** (1997) 166.

#### *Summary of revisions*

1. Isospin mixing and projection of the HF states has been implemented.
2. The finite-temperature formalism for the HFB equations has been implemented.
3. The Lipkin translational energy correction method has been implemented.
4. Calculation of the shell correction has been implemented.
5. The two-basis method for the solution to the HFB equations has been implemented.
6. The Augmented Lagrangian Method (ALM) for calculations with multiple constraints has been implemented.
7. The linear constraint method based on the cranking approximation of the RPA matrix has been implemented.
8. An interface between HFODD and the axially-symmetric and parity-conserving code HFBTHO has been implemented.
9. The mixing of the matrix elements of the HF or HFB matrix has been implemented.
10. A parallel interface using the MPI library has been implemented.
11. A scalable model for reading input data has been implemented.
12. OpenMP pragmas have been implemented in three subroutines.
13. The diagonalization of the HFB matrix in the simplex-breaking case has been parallelized using the ScaLAPACK library.
14. Several little significant errors of the previous published version were corrected.

#### *Restrictions on the complexity of the problem*

#### *Typical running time*

#### *Unusual features of the program*

The user must have access to (i) the NAGLIB subroutine F02AXE, or LAPACK subroutines ZHPEV, ZHPEVX, ZHEEVR, or ZHEEVD, which diagonalize complex hermitian matrices, (ii) the LAPACK subroutines DGETRI and DGETRF which invert arbitrary real matrices, (iii) the LAPACK subroutines DSYEVD, DSYTRF and DSYTRI which compute eigenvalues and eigenfunctions of real symmetric matrices and (iv) the LINPACK subroutines ZGEDI and ZGECO, which invert

arbitrary complex matrices and calculate determinants, (v) the BLAS routines DCOPY, DSCAL, DGEEM and DGEMV for double-precision linear algebra and ZCOPY, ZDSCAL, ZGEEM and ZGEMV for complex linear algebra, or provide another set of subroutines that can perform such tasks. The BLAS and LAPACK subroutines can be obtained from the Netlib Repository at the University of Tennessee, Knoxville: <http://netlib2.cs.utk.edu/>.

## LONG WRITE-UP

# 1 Introduction

The method of solving the Hartree-Fock (HF) equations in the Cartesian harmonic oscillator (HO) basis was described in the publication, Ref. [1]. Five versions of the code HFODD were previously published: (v1.60r) [2], (v1.75r) [3], (v2.08i) [4], (v2.08k) [5], and (v2.40h) [6]. The User's Guide for version (v2.40v) is available in Ref. [7] and the code home page is at <http://www.fuw.edu.pl/~dobaczew/hfodd/hfodd.html>. The present paper is a long write-up of the new version (v2.49t) of the code HFODD. This extended version features the isospin mixing and projection of the HF states, the finite-temperature formalism for the HF+BCS and HFB equations, and several other major modifications. It is also built upon a hybrid MPI/OpenMP parallel programming model which allows large-scale calculations on massively parallel computers. In serial mode, it remains fully compatible with all previous versions. Information provided in previous publications [2]-[6] thus remains valid, unless explicitly mentioned in the present long write-up.

In Section 2 we briefly review the modifications introduced in version (v2.49t) of the code HFODD. We distinguish between features implementing (i) new physics modeling capabilities, (ii) new numerical techniques and (iii) parallel computing methods. Section 3 lists all additional new input keywords and data values, introduced in version (v2.49t). In serial mode, the structure of the input data file remains the same as in the previous versions, see Section 3 of Ref. [2]. In parallel mode, two input files, with strictly enforced names, must be used: `hfodd.d` has the same keyword structure as all previous HFODD input files, with the restriction that not all keywords can be activated (see list in Sec. 3.3.1); `hfodd_mpiio.d` contains processor-dependent data, see Sec. 3.3.2.

## 2 Modifications introduced in version (v2.49t)

### 2.1 New Physics Features

#### 2.1.1 Isospin Mixing and Projection

The concept of isospin symmetry, having its roots in the approximate charge independence of the nucleon-nucleon interaction, was already introduced in nuclear physics in the 1930s by Heisenberg and Wigner [8, 9]. Throughout the years, it has proven to be extremely powerful and not abated by the presence of the Coulomb force – the main source of the isospin symmetry violation in nuclei – simply because the isovector and isotensor parts of the Coulomb force are

much weaker than the dominant, isospin symmetry preserving components of the Coulomb and strong interactions.

Apart from the explicit violation of the isospin symmetry due to the strong and, predominantly, Coulomb interactions, various approximate theoretical methods used in nuclear structure calculations are often the sources of unphysical violation of this symmetry by themselves [10, 11, 12, 13, 14]. This specifically concerns the Hartree-Fock and Kohn-Sham theories that employ independent-particle wave functions, which manifestly break the isospin symmetry in  $N \neq Z$  nuclei even for isospin-conserving interactions. The most prominent effects of this spontaneous isospin-symmetry-breaking occur, however, in the ground-state configuration of odd-odd  $N = Z$  nuclei and in  $T \neq 0$  excited configurations of  $N = Z$  nuclei, see Ref. [14] and references cited therein. Hence, practical implementation of the method requires the isospin projection and subsequent re-diagonalization of the entire Hamiltonian in the isospin-projected basis. These two major building blocks of the isospin projection method will be described below. The discussion will be followed by a short presentation of the extended version of our model including the isospin and angular-momentum projections which is needed for specific applications including calculation of the isospin-symmetry breaking corrections to superallowed  $\beta$ -decay [15, 16, 17].

**The isospin projection:** To remove the unphysical isospin-symmetry violation introduced by the mean-field (MF) approximation, the code HFODD (v2.49t) was equipped with a new tool allowing for the isospin projection after variation of an arbitrary symmetry-unrestricted Slater determinant  $|\Phi\rangle$  provided by the code. The method implemented uses the standard one-dimensional isospin-projection operator  $\hat{P}_{T_z T_z}^T$ :

$$|TT_z\rangle = \frac{1}{\sqrt{N_{TT_z}}} \hat{P}_{T_z T_z}^T |\Phi\rangle = \frac{2T+1}{2\sqrt{N_{TT_z}}} \int_0^\pi d\beta_T \sin \beta_T d_{T_z T_z}^T(\beta_T) \hat{R}(\beta_T) |\Phi\rangle, \quad (1)$$

which allows for decomposing the Slater determinant  $|\Phi\rangle$ ,

$$|\Phi\rangle = \sum_{T \geq |T_z|} b_{TT_z} |TT_z\rangle, \quad (2)$$

into good-isospin basis  $|TT_z\rangle$ . Here,  $\beta_T$  denotes the Euler angle associated with the rotation operator  $\hat{R}(\beta_T) = e^{-i\beta_T \hat{T}_y}$  about the  $y$ -axis in the isospace,  $d_{T_z T_z}^T(\beta_T)$  is the Wigner function [18], and  $T_z = (N - Z)/2$  is the third component of the total isospin  $T$ . The normalization factors  $N_{TT_z}$ , or interchangeably the expansion coefficients  $b_{TT_z}$ , read:

$$N_{TT_z} \equiv |b_{TT_z}|^2 = \langle \Phi | \hat{P}_{T_z T_z}^T | \Phi \rangle = \frac{2T+1}{2} \int_0^\pi d\beta_T \sin \beta d_{T_z T_z}^T(\beta_T) \mathcal{N}(\beta_T), \quad (3)$$

where

$$\mathcal{N}(\beta_T) = \langle \Phi | \hat{R}(\beta_T) | \Phi \rangle \quad (4)$$

stands for the overlap kernel.

The isospin projection operator is used to construct a subspace (basis) of good-isospin states  $|TT_z\rangle$ . Its size is controlled by the parameter  $\varepsilon_T$ , such that only the states  $|TT_z\rangle$  that have tangible contributions,  $|b_{TT_z}|^2 \geq \varepsilon_T$ , to the MF state are retained for further re-diagonalization. In practice,  $\varepsilon_T = 10^{-10}$  sets the limit of  $T \leq |T_z| + 5$ . The good-isospin basis created in this

way, although of rather small dimension, is believed to capture the right balance between the short-range strong interaction and the long-range Coulomb force (see discussion in Ref. [13]). The parameter  $\varepsilon_T = 10^{-10}$  also ensures that the two basic quantities reflecting the accuracy of the method, namely, the overlap (normalization) sum rule,

$$\sum_{T \geq |T_z|} |b_{TT_z}|^2 = 1, \quad (5)$$

and total MF energy sum rule,

$$E_{MF} \equiv \langle \Phi | \hat{H} | \Phi \rangle = \sum_{TT' \geq |T_z|} b_{T'T_z}^* b_{TT_z} \langle T'T_z | \hat{H} | TT_z \rangle, \quad (6)$$

are both fulfilled with extremely high accuracy. The latter property is due to the fact that the isospin-projection method is practically free from divergences plaguing particle-number and angular-momentum [19, 20, 21, 22] methods. An analytical proof of this rather remarkable feature of the isospin projection is given in Ref. [14].

**Rediagonalization in the isospin projected basis:** Expansion coefficients  $b_{T,T_z}$  do not reflect the physical isospin mixing. Indeed, they are affected by the spurious isospin mixing, which is due to the spontaneous breaking of the isospin symmetry caused by the MF approximation. To calculate the true isospin mixing, one needs to rediagonalize the total nuclear Hamiltonian in the good-isospin basis  $|TT_z\rangle$ . The present implementation of the code HFODD admits Hamiltonians that include the isoscalar part of the kinetic energy  $\hat{T}$ , isospin-invariant Skyrme functional,  $\hat{V}^S$ , and Coulomb force,  $\hat{V}^C$ ; the latter can further be decomposed into the isoscalar,  $\hat{V}_{00}^C$ , isovector,  $\hat{V}_{10}^C$ , and isotensor,  $\hat{V}_{20}^C$ , components, that is,

$$\hat{H} = \hat{T} + \hat{V}^S + \hat{V}^C \equiv \hat{T} + \hat{V}^S + \hat{V}_{00}^C + \hat{V}_{10}^C + \hat{V}_{20}^C, \quad (7)$$

where

$$\hat{V}_{00}^C(r_{ij}) = \frac{1}{4} \frac{e^2}{r_{ij}} \left( 1 + \frac{1}{3} \hat{\tau}^{(i)} \circ \hat{\tau}^{(j)} \right), \quad (8)$$

$$\hat{V}_{10}^C(r_{ij}) = -\frac{1}{4} \frac{e^2}{r_{ij}} \left( \hat{\tau}_{10}^{(i)} + \hat{\tau}_{10}^{(j)} \right), \quad (9)$$

$$\hat{V}_{20}^C(r_{ij}) = \frac{1}{4} \frac{e^2}{r_{ij}} \left( \hat{\tau}_{10}^{(i)} \hat{\tau}_{10}^{(j)} - \frac{1}{3} \hat{\tau}^{(i)} \circ \hat{\tau}^{(j)} \right). \quad (10)$$

Note, that the components  $\hat{V}_{\lambda 0}^C$  are constructed by coupling the spherical components of the one-body isospin operator:

$$\hat{\tau}_{10} = \hat{\tau}_z, \quad \hat{\tau}_{1\pm 1} = \mp \frac{1}{\sqrt{2}} (\hat{\tau}_x \pm i\hat{\tau}_y), \quad (11)$$

where  $\hat{\tau}_i$ ,  $i = x, y, z$  denote Pauli matrices and symbol  $\circ$  stands for the scalar product of isovectors. Hence, from a mathematical viewpoint, they represent isoscalar, covariant rank-1 (isovector), and covariant rank-2 axial (isotensor) spherical tensor components of the Coulomb interaction, respectively. This mathematical property allows the use of Racah algebra in order to

calculate matrix elements of the Hamiltonian. The rather lengthy details concerning this specific theoretical aspect of our model are given in Ref. [14] and will not be repeated here.

Radiagonalization of the total Hamiltonian in the good-isospin basis leads to the eigenstates:

$$|n, T_z\rangle = \sum_{T \geq |T_z|} a_{TT_z}^n |TT_z\rangle, \quad (12)$$

numbered by index  $n$ . Apart of the eigenenergies  $E_{n, T_z}$  and the amplitudes  $a_{TT_z}^n$  that define the degree of isospin mixing, the code also provides the so-called isospin (Coulomb) mixing coefficients or, equivalently, the isospin impurities. For the  $n$ -th eigenstate, the isospin impurity is defined as  $\alpha_C^n = 1 - |a_{TT_z}^n|_{\max}^2$ , where  $|a_{TT_z}^n|_{\max}^2$  stands for the squared norm of the dominant amplitude in the wave function  $|n, T_z\rangle$ , and is given in percents.

Evaluation of the isospin impurity  $\alpha_C$  is a prerequisite for determining the isospin-breaking corrections  $\delta_C$  to the  $0^+ \rightarrow 0^+$  Fermi matrix element of the isospin raising/lowering operator  $\hat{T}_{\pm}$ . Of particular interest in nuclear physics are the Fermi matrix elements:

$$|\langle I = 0, T \approx 1, T_z = \pm 1 | \hat{T}_{\pm} | I = 0, T \approx 1, T_z = 0 \rangle|^2 \equiv 2(1 - \delta_C), \quad (13)$$

for a set of nuclei undergoing the super-allowed beta decay, because the  $\delta_C$  parameter is the key nuclear quantity needed for precise nuclear tests of the conserved-vector-current hypothesis and for the determination of the up-down matrix element in the Cabibbo-Kobayashi-Maskawa matrix (see Ref. [23] and references quoted therein). The calculation of the Fermi matrix elements (13) was one of the primary motivations to couple the newly developed isospin projection with the existing angular-momentum projection [6]. Indeed, such a four-dimensional projection appears to be absolutely necessary to get reliable representation of decaying states in daughter (parent)  $|I = 0, T \approx 1, T_z = \pm 1\rangle$  and parent (daughter)  $|I = 0, T \approx 1, T_z = 0\rangle$  nuclei undergoing the super-allowed transition, respectively (see Ref. [15]). It should be stressed, however, that the range of applicability of the four-dimensional projection is by no means limited to the computation of matrix elements (13) but also encompasses, in particular, various applications in high-spin physics in  $N \sim Z$  nuclei.

**The four-dimensional isospin and angular momentum projection:** The implementation of the four-dimensional projection follows rather closely the angular-momentum projection scheme adopted in version (v2.40h) of the code and described in detail in Ref. [6] (cf. Refs. [22, 24]). Hence, in the following, we will refrain from technicalities and concentrate on discussing the main building blocks of the method. The starting point is the good angular momentum  $I$  and good isospin  $T$  basis generated by acting with standard angular-momentum  $\hat{P}_{MK}^I$  and isospin  $\hat{P}_{T_z T_z}^T$  projectors on the Slater determinant  $|\Phi\rangle$ :

$$|IMK; TT_z\rangle = \hat{P}_{T_z T_z}^T \hat{P}_{MK}^I |\Phi\rangle, \quad (14)$$

where  $M$  and  $K$  stand for the angular-momentum projections along the laboratory and intrinsic  $z$ -axes, respectively. The basis composed of states  $|IMK; TT_z\rangle$  is over-complete. This problem is overcome by constructing, separately for each  $I$  and  $T$ , the so-called collective subspace spanned by the natural states:

$$|IM; TT_z\rangle^{(m)} = \frac{1}{\sqrt{n_m}} \sum_K \eta_K^{(m)} |IMK; TT_z\rangle. \quad (15)$$

The  $m^{\text{th}}$  natural state is constructed by using the mixing amplitudes  $\eta_K^{(m)}$  that correspond to the  $m^{\text{th}}$  eigenstate of the norm matrix, see Eq. (9) in [6]:

$$\sum_{K'} N_{KK'}^{TT_z} \eta_{K'}^{(m)} = n_m \eta_K^{(m)}. \quad (16)$$

Only the eigenstates corresponding to eigenvalues  $n_m > \zeta$  are taken into account, with the basis cut-off parameter  $\zeta$  introduced in Ref. [6]. In this way, for each value of the angular momentum  $I$  and isospin  $T$ , the collective subspace contains  $m_{\text{max}}(I, T)$  states. The overlap matrix appearing in Eq. (16) reads:

$$\begin{aligned} N_{KK'}^{TT_z} &= \langle \Phi | \hat{P}_{T_z T_z}^T \hat{P}_{KK'}^I | \Phi \rangle = \\ &= \frac{(2I+1)(2T+1)}{16\pi^2} \int d\beta_T d_{T_z T_z}^T(\beta_T) \int d\Omega D_{KK'}^{I*}(\Omega) \langle \Phi | \hat{R}(\beta_T) \hat{R}(\Omega) | \Phi \rangle, \end{aligned} \quad (17)$$

where  $\hat{R}(\Omega) = e^{-i\alpha\hat{I}_z} e^{-i\beta\hat{I}_y} e^{-i\gamma\hat{I}_z}$  stands for the space-rotation operator, which depends on three Euler angles  $\Omega = (\alpha, \beta, \gamma)$ , and  $D_{KK'}^I(\Omega)$  is the Wigner function.

To simultaneously take into account the  $K$ -mixing and isospin mixing, the code performs, separately for each value of the angular momentum  $I$ , the full diagonalization of the total Hamiltonian (7) in the  $n(I)$ -dimensional,  $n(I) = \sum_{T \geq |T_z|} m_{\text{max}}(I, T)$ , collective space spanned by natural states (15). Such a diagonalization leads to the eigenstates of the form:

$$|n; IM; T_z\rangle = \sum_{T \geq |T_z|} \sum_{m=1}^{m_{\text{max}}(I, T)} a_{mT}^{(n)}(I) |IM; TT_z\rangle^{(m)}, \quad (18)$$

which are labeled by the conserved quantum numbers  $I, M$ , and  $T_z = (N - Z)/2$ , and by the additional index  $n$ , which characterizes the  $K$  and isospin mixing. For the sake of completeness, it is worth mentioning that the code also provides the  $K$ -mixed and isospin-conserving eigenstates, which result from the diagonalization of the total Hamiltonian with all isospin-symmetry-breaking ( $\Delta T \neq 0$ ) matrix elements set to zero.

### 2.1.2 Finite-temperature Formalism

The equilibrium state of a physical system at constant temperature  $T$  and chemical potential  $\lambda$  is obtained from the minimization of the grand canonical potential  $\Omega$  [25, 26, 27, 28, 29]

$$\Omega = E - TS - \lambda N, \quad (19)$$

where the energy ( $E$ ), entropy ( $S$ ) and particle-number ( $N$ ) are statistical averages and are given by

$$E = \text{Tr}(\hat{\mathcal{D}}\hat{H}), \quad (20)$$

$$S = -k\text{Tr}(\hat{\mathcal{D}}\ln\hat{\mathcal{D}}), \quad (21)$$

$$N = \text{Tr}(\hat{\mathcal{D}}\hat{N}). \quad (22)$$

The density operator  $\hat{\mathcal{D}}$  and the grand partition function  $\mathcal{Z}$  are defined, respectively, as

$$\hat{\mathcal{D}} = \frac{1}{\mathcal{Z}} e^{-\beta(\hat{H}-\lambda\hat{N})}, \quad (23)$$

$$\mathcal{Z} = \text{Tr} \left[ e^{-\beta(\hat{H}-\lambda\hat{N})} \right], \quad (24)$$

where  $\beta = 1/kT$  and  $\hat{H}$  is the two-body Hamiltonian. In the MF approximation, the two-body density operator in Eq. (23) is replaced by a one-body operator. It has been demonstrated in [25] that the variation of the grand canonical potential with respect to the density operator  $\hat{\mathcal{D}}$  leads to HFB equations that are formally equivalent to the  $T = 0$  equations, namely

$$\begin{pmatrix} h - \lambda & \Delta \\ -\Delta^* & -h^* + \lambda \end{pmatrix} \begin{pmatrix} U_\mu \\ V_\mu \end{pmatrix} = E_\mu \begin{pmatrix} U_\mu \\ V_\mu \end{pmatrix}, \quad (25)$$

where  $h$  and  $\Delta$  are the Hartree-Fock and pairing potentials, and are obtained from the energy density functional as usual. The inclusion of finite temperature in the formalism is achieved by generalizing the expression of the density matrix and pairing tensor. In configuration space, they read [29]

$$\rho = UfU^\dagger + V^*(1-f)V^T, \quad (26)$$

$$\kappa = UfV^\dagger + V^*(1-f)U^T, \quad (27)$$

where the quantity “ $f$ ” stands for the Fermi function, defined as,

$$f_\mu = \frac{1}{1 + e^{\beta E_\mu}}, \quad (28)$$

with  $E_\mu$  the  $\mu^{\text{th}}$  quasi-particle energy. In coordinate space, their expression becomes

$$\rho(\mathbf{r}\sigma, \mathbf{r}'\sigma') = \sum_{0 \leq E_\mu \leq E_{\text{max}}} \{ f_\mu U^{(\mu)}(\mathbf{r}\sigma) U^{(\mu)*}(\mathbf{r}'\sigma') + (1 - f_\mu) V^{(\mu)*}(\mathbf{r}\sigma) V^{(\mu)}(\mathbf{r}'\sigma') \}, \quad (29)$$

$$\kappa(\mathbf{r}\sigma, \mathbf{r}'\sigma') = \sum_{0 \leq E_\mu \leq E_{\text{max}}} \{ f_\mu U^{(\mu)}(\mathbf{r}\sigma) V^{(\mu)*}(\mathbf{r}'\sigma') + (1 - f_\mu) V^{(\mu)*}(\mathbf{r}\sigma) U^{(\mu)}(\mathbf{r}'\sigma') \}. \quad (30)$$

All additional densities (kinetic, spin-current, etc.) are derived from the particle density (29). In HFODD, the conventional pairing tensor is replaced by the pairing density  $\tilde{\rho}(\mathbf{r}\sigma, \mathbf{r}'\sigma')$  obtained according to:  $\tilde{\rho}(\mathbf{r}\sigma, \mathbf{r}'\sigma') = -2\sigma'\kappa(\mathbf{r}\sigma, \mathbf{r}' - \sigma')$ , see [30].

The code HFODD implements the finite-temperature formalism in the HFB and HF+BCS modes. For the latter case, we refer to Sec. 5 of [25] for the details of the expressions coded. For the former case, we would like to emphasize that the calculation of the Fermi level  $\lambda$  needs to be modified at  $T > 0$ . Let us recall that the adjustment of  $\lambda$  in HFODD is based on BCS formula [30]: given the equivalent spectrum of single-particle (s.p.) states  $\varepsilon_\mu$  and pairing gaps  $\Delta_\mu$ , the particle number is computed according to:

$$N = \sum_{\mu} [v_\mu^2 + (u_\mu^2 - v_\mu^2)f_\mu], \quad (31)$$

with the Fermi functions  $f_\mu$  of Eq. (28) and the occupation factors given by:

$$v_\mu^2 = \frac{1}{2} \left[ 1 - \frac{\varepsilon_\mu - \lambda}{E_\mu^{\text{BCS}}} \right], \quad u_\mu^2 = 1 - v_\mu^2, \quad (32)$$

with  $E_\mu^{\text{BCS}} = \sqrt{(\varepsilon_\mu - \lambda)^2 + \Delta_\mu^2}$ . When applying the Newton-Raphson method to determine  $\lambda$  by the condition that  $N = N_0$ , the implicit dependence of the  $f_\mu$  on  $\lambda$  must be taken into account. This is done by updating the  $f_\mu$  at each  $\lambda$  according to:

$$f_\mu(\lambda) = \frac{1}{1 + e^{\beta E_\mu^{\text{BCS}}}}, \quad (33)$$

and introducing the corresponding additional term  $\partial f_\mu / \partial \lambda$  in the derivative  $\partial N / \partial \lambda$ . The contribution from the thermal occupation factors is crucial for the convergence in the unpaired regime. Note that in the case of zero-range pairing interactions, there can be stability issues for low cut-offs near the phase transition. Recently, the finite temperature extension of HFODD has been used in a systematic study of fission paths and barriers of actinide and superheavy elements [31, 32].

### 2.1.3 Lipkin Translational Energy Correction

According to the Lipkin method [33, 34], the linear-momentum projected energy of a system at rest can be calculated without the actual projection as:

$$E_\Phi(0) = \langle \Phi | \hat{H} - \hat{K} | \Phi \rangle, \quad (34)$$

where  $\hat{H}$  is the two-body effective Hamiltonian and

$$\hat{K} = k \hat{\mathbf{P}}^2 \quad (35)$$

is the Lipkin operator in the quadratic approximation,  $\hat{\mathbf{P}} = \sum_{i=1}^A \hat{\mathbf{p}}_i$  is the total linear momentum operator and  $k$  is a parameter to be determined. The optimum state is found by minimizing the right hand side of Eq. (34). Note that the projected energy depends parametrically on the parameter  $k$ , that is, there is no variation with respect to  $k$  (no contribution to the HF potentials).

To determine the value of  $k$ , we proceed as follows [33, 34]. First define at each iteration the translated wave-function  $|\Phi(\mathbf{R})\rangle$  as:

$$|\Phi(\mathbf{R})\rangle = e^{\frac{i}{\hbar} \mathbf{R} \cdot \hat{\mathbf{P}}} |\Phi\rangle. \quad (36)$$

Then one can show that the correcting Lipkin parameter  $k$  reads:

$$k = \frac{h(\mathbf{R}) - h(\mathbf{0})}{p_2(\mathbf{R}) - p_2(\mathbf{0})}, \quad (37)$$

where:

$$h(\mathbf{R}) = \frac{\langle \Phi | \hat{H} | \Phi(\mathbf{R}) \rangle}{\langle \Phi | \Phi(\mathbf{R}) \rangle}, \quad p_2(\mathbf{R}) = \frac{\langle \Phi | \hat{\mathbf{P}}^2 | \Phi(\mathbf{R}) \rangle}{\langle \Phi | \Phi(\mathbf{R}) \rangle}, \quad (38)$$

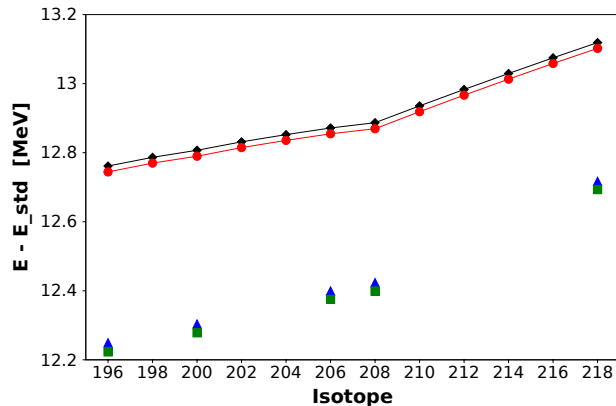


Figure 1: Lipkin projected energies (34) relative to the standard SLY4 energies, calculated for the chain of lead isotopes. The results for the exact masses (Lipkin operator (35) with  $k = k_0$  of Eq. (39)) are given with the center-of-mass correction added after (diamonds) and before (circles) variation. Similarly, for the renormalized masses ( $k$  of Eq. (37)), the results for closed sub-shells are given with the correction added after (triangles) and before (squares) variation.

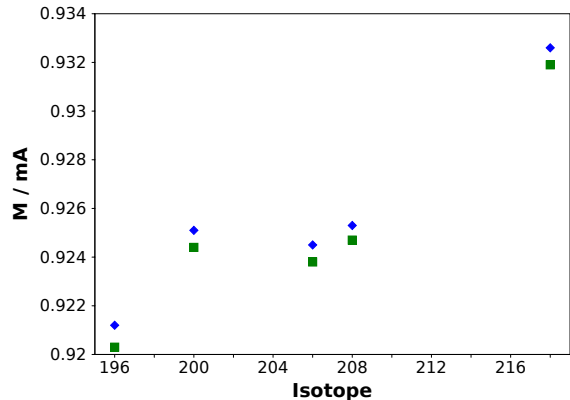


Figure 2: Ratios  $k_0/k = M/mA$  of the renormalized and exact masses determined after (triangles) and before (squares) variation.

are the energy and momentum kernels. The calculation of  $k$  at each iteration is therefore straightforward, since it only requires to compute  $h(\mathbf{R})$  and  $p_2(\mathbf{R})$  for a single (arbitrary) value of the shift vector  $\mathbf{R}$ . The parameter  $k$  plays the role of a renormalized mass. It can be compared to the traditional so-called 1-body center-of-mass correction factor:

$$k_0 = \frac{\hbar^2}{2mA} \quad (39)$$

where  $m$  is the nucleon mass. Since for the translational-symmetry restoration the Gaussian Overlap Approximation (GOA) is excellent [34], one can also approximate the Lipkin parameter by the GOA expression [35, 34]:

$$k_{\text{GOA}} = -\frac{h(\mathbf{R}) - h(\mathbf{0})}{4 \log^2(\langle \Phi | \Phi(\mathbf{R}) \rangle)} \mathbf{R}^2, \quad (40)$$

where one assumes that  $h(\mathbf{R})$  and  $\log(\langle \Phi | \Phi(\mathbf{R}) \rangle)$  can be at the shift of  $\mathbf{R}$  approximated by a parabola. The GOA expression is much faster to evaluate, because it does not require calculating kernels of the two-body operator  $\hat{\mathbf{P}}^2$ .

Figures 1–2 illustrate various aspects of the Lipkin method for linear momentum projection. In the captions of the figures, the term 'exact mass' refer to the quantity  $k_0$ , and the term 'renormalized mass' to the quantity  $k$ .

### 2.1.4 Shell Correction

The shell-correction method relies on the Strutinsky energy theorem, which states that the total energy  $E$  of the nucleus reads:

$$E = E_{\text{bulk}} + \delta R_{\text{shell}}, \quad (41)$$

where  $E_{\text{bulk}}$  varies slowly with proton and neutron numbers, and  $\delta R_{\text{shell}}$  is a rapidly varying function of  $Z$  and  $N$  that captures the quantum corrections to the liquid drop [36, 37]. It was demonstrated in [38] that such a simple decomposition remains valid when the total energy  $E$  is computed microscopically as the integral of some energy density functional or expectation value of a two-body effective Hamiltonian at the Hartree-Fock approximation.

The shell correction must be computed from a set of s.p. levels  $\{e_i\}$ , which in HFODD are the Hartree-Fock s.p. energies. In its traditional form, it is given by:

$$\delta R_{\text{shell}}^{(1)} = \sum_{i \in \{\text{occ}\}} e_i - \left\langle \sum_i e_i \right\rangle_{\text{smooth}}, \quad (42)$$

where  $i \in \{\text{occ}\}$  represents a set of occupied states (for the HF vacuum, this is the set of the lowest  $Z$  or  $N$  levels), and the bracket  $\langle \dots \rangle_{\text{smooth}}$  represents the Strutinsky smoothing procedure. For the latter, we follow the prescription presented in [39] and applied on a large scale in macroscopic-microscopic calculations, e.g., in [40].

The smoothed energy in expression (42) contains a spurious contribution from positive energy states  $e_i > 0$  which can become problematic when approaching the dripline. This spurious term can be removed by subtracting to Eq. (42) the smooth energy obtained for an independent gas of particles [41, 42]. This leads to slightly different prescription  $\delta R_{\text{shell}}^{(2)}$  for the shell correction:

$$\delta R_{\text{shell}}^{(2)} = \sum_{i \in \{\text{occ}\}} e_i - \left\{ \left\langle \sum_i e_i \right\rangle_{\text{smooth}} - \left\langle \sum_i t_i \right\rangle_{\text{smooth}} \right\}, \quad (43)$$

where the  $t_i$  are the eigenvalues of the kinetic energy operator. The shell correction is computed twice, for protons and neutrons. For protons, the Coulomb potential must also be taken into account by doing the substitution  $t_i \rightarrow (\hat{t} + \hat{V}_{\text{Cou}})_i$ . The shell correction (43) is of course evaluated at the convergence of the self-consistent HF calculation. Both estimates  $\delta R_{\text{shell}}^{(1)}$  and  $\delta R_{\text{shell}}^{(2)}$  of the shell correction are available in HFODD and are triggered by the value of the input parameter IFSHEL.

## 2.2 New Numerical Features

### 2.2.1 Two-basis Method for HFB Calculations

The two-basis method was devised in Ref. [43] to solve the HFB equations in spatial coordinates. The method allows for decoupling the particle-hole and particle-particle channels from one another and using the same technology as that developed for the HF+BCS method, even for the complete HFB problem. The essence of the method relies on the solution of the HFB equations in the basis of eigenstates of the particle-hole MF operator  $h$ . In spatial coordinates, this operator is not diagonalized in every iteration, but a set of eigenfunctions is evolved in imaginary time,

and thus they converge to eigenstates only at the end of the iterative process. In our case, the self-consistent equations are solved by using the HO basis and the imaginary-time evolution is not used; therefore, we implement the two-basis method by explicitly diagonalizing  $h$ .

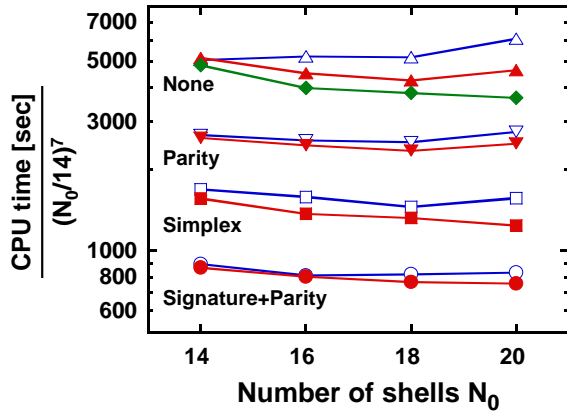


Figure 3: CPU times required to perform five HFB iterations for conserved signature and parity (circles), conserved simplex (squares), conserved parity (down-triangles), and with no conserved symmetry (up-triangles). Standard HFB method (open symbols) is compared with requesting the diagonalization subroutine to return only the eigenvectors below the cutoff energy (full symbols). The diamonds show the results obtained within the two-basis method implemented for the case of no conserved symmetry.

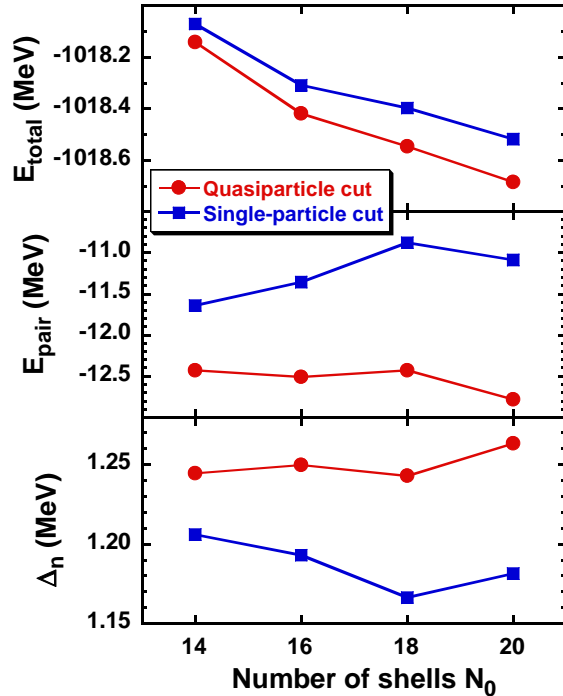


Figure 4: The HFB results obtained within the standard method corresponding to the cutoff in the quasiparticle space (circles) and within the two-basis method corresponding to the cutoff in the s.p. space (squares).

This procedure has two advantages over the standard HFB method. First, the cutoff of the configuration space can now be performed in the s.p. space and not in the quasiparticle space. Therefore, the dimension of the HFB equations, reduced to s.p. states with energies  $\epsilon$  below the cutoff energy,  $\epsilon \leq \bar{\epsilon}_{\max}$ , is much smaller than the full HO space. This speeds up the calculations. Second, HFB calculations in a reduced s.p. space do not suffer from formal drawbacks related to the cutoff in the quasiparticle space, see discussion in Ref. [44].

Figure 3 shows the CPU times required to perform the HFB calculations for  $^{120}\text{Sn}$  by using the cutoff energy of  $E_{\text{cut}} = 60$  MeV, Skyrme functional SLY4, and pairing-force parameters of Eq. (14) in Ref. [4],  $V_0 = -285.88$  MeV,  $\rho_0 = 0.32$  fm $^{-3}$ , and  $\alpha = 1$ . The results were obtained for bases of  $N_0 = 14$ –20 and for four conserved-symmetry conditions, as indicated in the Figure. The CPU times scale as  $N_0^7$ . It turns out that in the case of calculations performed without any conserved symmetry, the two-basis method can be up to 30% faster than the standard HFB method. However, almost half of this gain can be obtained by simply requesting in the standard HFB method that the HFB wave functions be calculated only below the quasiparticle cutoff energy (see keyword `CUT_SPECTR`). In view of this limited gain in the CPU time, in version

(v2.49t) the two-basis method is not implemented in the remaining three conserved-symmetry conditions.

The two-basis method gives results that are close, but not identical, to those given by the standard HFB method. This is illustrated in Figure 4, where the total energies (upper panel) can differ up to 200 keV, the pairing energies (middle panel) up to 1.5 MeV, and the neutron pairing gaps (bottom panel) up to 70 keV. Although these differences are non-negligible, they are probably inferior to other uncertainties of the approach, and at present the physical advantages or disadvantages of one method over the other cannot be established. One should stress that the two methods of implementing the cutoff give exactly the same numbers of quasiparticles, so the above difference are not caused by different sizes of the model spaces.

## 2.2.2 Augmented Lagrangian Method

Multi-constrained EDF calculations are a crucial ingredient of a number of nuclear structure applications. The microscopic description of high-spin states is based on the cranking model, which requires a constraint on the value of the total angular momentum. Modeling the fission process involves the calculation of multi-dimensional potential energy surfaces, where the constraints are imposed on expectation values of the multipole moments. Most generally, beyond-mean-field applications, or multi-reference EDF, rely on a basis of constrained MF states used to generate collective motion.

In previous versions of HFODD, constraints on the nuclear shape took the standard quadratic form, see Eq. (22) in [1]. This so-called quadratic penalty method was chosen to avoid the pitfalls of the method of Lagrange multipliers (linear constraints), which often fails to converge. The quadratic penalty method is usually very fast and robust, but does not always yield the desired solution: the expectation value of the multipole moments at convergence may differ, sometimes significantly, from the requested values. In addition, it depends rather sensitively on the stiffness parameter, which controls the magnitude of the corrective term.

The Augmented Lagrangian Method (ALM) provides a valuable alternative for multi-constrained calculations [45, 46]. It is a general algorithm which aims at minimizing a scalar function  $\mathcal{E}(\mathbf{x})$  of the vector  $\mathbf{x}$  under a set of constraints  $g_i(\mathbf{x}) = q_i^0$  (the so-called finite-dimensional, equality-constrained nonlinear optimization problem). In practice, it can simply be viewed as a smart combination of both the linear and quadratic penalty methods. Adopting the same notations as in Sec. 2.3 of [1], the total energy takes the form:

$$\mathcal{E}' = \mathcal{E} - \sum_{\lambda\mu} L_{\lambda\mu} (\langle \hat{Q}_{\lambda\mu} \rangle - \bar{Q}_{\lambda\mu}) + \sum_{\lambda\mu} C_{\lambda\mu} (\langle \hat{Q}_{\lambda\mu} \rangle - \bar{Q}_{\lambda\mu})^2, \quad (44)$$

where  $L_{\lambda\mu}$  is the Lagrange parameter for the multipole  $(\lambda, \mu)$ ,  $C_{\lambda\mu}$  is the corresponding stiffness and  $\bar{Q}_{\lambda\mu}$  the requested value for the multipole moment  $\hat{Q}_{\lambda\mu}$ . Note that the minus sign for the linear constraint term is a matter of convention. While the stiffness is an input parameter that remains constant along the iterations,  $L_{\lambda\mu}$  has to be re-adjusted. At iteration  $m + 1$ , the new Lagrange parameter reads:

$$L_{\lambda\mu}^{(m+1)} = L_{\lambda\mu}^{(m)} - 2C_{\lambda\mu} (\langle \hat{Q}_{\lambda\mu} \rangle^{(m)} - \bar{Q}_{\lambda\mu}). \quad (45)$$

For a EDF solver already implementing the quadratic penalty method, adding the ALM is extremely simple: (i) The linear term in Eq. (44) must be added to the total energy, (ii) the

matrix elements of the corresponding HF potential  $U^{(m)} = -\sum_{\lambda\mu} L_{\lambda\mu}^{(m)} \hat{Q}_{\lambda\mu}$  must be added to the HF(B) matrix, and (iii) the Lagrange parameter must be updated at every iteration according to Eq. (45). The method induces almost no computational overhead, is very robust, and always gives very precisely the requested solution, see [47].

### 2.2.3 Linear Constraints Based on the RPA Matrix

The ALM method does not make any specific hypotheses as to how the function  $\mathcal{E}(\mathbf{x})$  is computed. Within the nuclear EDF, the function  $\mathcal{E}(\mathbf{x})$  is the total energy of the nucleus, and is itself obtained as the solution to a variational problem. One may therefore take advantage of this additional information to adapt the standard optimization algorithm with linear constraints. Such an approach was proposed already 30 years ago in the context of the self-consistent nuclear MF theory with finite range effective forces [48]. At every iteration, an estimate of the QRPA matrix at the cranking approximation is computed. This information is used to make an educated update of the Lagrange parameters  $L_{\lambda\mu}$  of the linear constraints. A detailed and pedagogical presentation of the algorithm and its applications for fission barriers calculations can be found in [49].

The implementation of the method in HFODD follows very closely the Appendix A of [49], and we refer to this work for further information. Let us note that this method requires the matrix of the constraint operator in the q.p. basis, which involves 8 matrix multiplications per iteration (4 for neutrons, 4 for protons). The computation of the constraints correlation matrix also requires  $N_c^2$  additional matrix multiplications per iteration, where  $N_c$  is the number of constraints. When simplex symmetry is conserved, the properties of the basis in HFODD reduce the size of the matrices involved in all these operations to one half of the total basis size at most. The computation overhead can still be noticeable, but is always largely compensated by a drastic reduction in the number of iterations necessary to reach convergence and the near-perfect precision of the obtained solution. All major linear algebra operations (matrix multiplication and inversion) are carried out by BLAS and LAPACK routines.

### 2.2.4 Interface with HFBTHO

The code HFBTHO solves the Skyrme HFB equations in the HO basis by assuming axial and reflection symmetry [50]. These built-in symmetries make the HFB matrix block-diagonal, and the typical run time of the program is at least an order of magnitude shorter than for HFODD. This makes HFBTHO an ideal tool for large-scale calculations in cases where axial- and reflection symmetries are sensible assumptions [51]. Conversely, HFBTHO is not appropriate for specific problems such as the description of nuclear fission, where the complexity of the nuclear shapes impose the use of a fully symmetry-unrestricted solver like HFODD.

Both codes have been carefully benchmarked against one another in even-even [52] and odd nuclei [53] at the equal-filling approximation. The difference of total energies in a nucleus like  $^{120}\text{Sn}$  is typically of the order of 10 eV, and can entirely be attributed to the different techniques of computing the Coulomb potential. Such a nearly perfect match makes it possible to accelerate HFODD run time by coupling the two codes together: for a given nucleus, the calculation is first carried out by HFBTHO (assuming axial and reflection symmetry), then restarted with HFODD after a simple unitary transformation. If the physical solution is axial and parity invariant, the HFBTHO solution is the correct one, and HFODD can stop after the basis transformation.

If the solution breaks any of these symmetries, the self-consistent procedure will continue until convergence. The motivation for such an interface is the observation that, for nearly all nuclear shapes, the driving deformation is the axial quadrupole moment  $Q_{20}$ .

Let us denote by  $\{|SIM_n\rangle\} \equiv \{|n_x, n_y, n_z; s = \pm i\rangle\}$  the simplex-conserving Cartesian Harmonic Oscillator basis used in HFODD. We denote by  $\{|CYL_n\rangle\}$  the cylindrical harmonic oscillator basis used in HFBTHO,  $|CYL_n\rangle \equiv |N, n_\rho, n_z, \Lambda, \Omega\rangle$ . The basis transformation  $\{|CYL_n\rangle\} \rightarrow \{|SIM_n\rangle\}$  proceeds in two steps:

1. The coordinate transformation  $\{|CYL_n\rangle\} \rightarrow \{|CAR_n\rangle\}$  is carried out, where the  $\{|CAR_n\rangle\} \equiv |n_x, n_y, n_z; \sigma\rangle$  are the Cartesian harmonic oscillator states and  $\sigma = \pm 1/2$  is the  $z$ -projection of the intrinsic spin;
2. A unitary phase transformation is then performed to go to the good  $y$ -simplex basis:  $\{|CAR_n\rangle\} \rightarrow \{|SIM_n\rangle\}$ .

**Coordinate transformation** - The spatial quantum numbers in Cartesian and cylindrical coordinates are related through:

$$N = n_x + n_y + n_z = 2n_\rho + \Lambda + n_z. \quad (46)$$

Let us note  $n_\perp = N - n_z$ . In principle:

$$0 \leq n_\rho \leq n_\perp, \quad \text{and} \quad -n_\perp \leq \Lambda \leq +n_\perp. \quad (47)$$

However, quantum numbers  $\Lambda < 0$  (therefore  $n_\rho > n_\perp/2$ ) correspond to states which are the time-reversed partners of the states  $\Lambda > 0$ : In HFBTHO, time-reversal symmetry is conserved, all basis states with  $\Lambda < 0$  are disregarded, and the HFB matrix  $\mathcal{H}$  is explicitly block-diagonal by  $\Omega = \Lambda \pm \sigma$  values. The full HFB matrix is therefore reconstructed from each  $\Omega$ -block. By a suitable reordering of indexes, it is then split into 4 matrices  $\mathcal{H}^{(\sigma\sigma')}$ . The  $\mathcal{H}^{(\sigma\sigma')}$  are purely spatial matrices with matrix elements of the type:

$$\langle n'_x \Lambda' n'_z | \hat{\mathcal{H}}^{(\sigma\sigma')} | n_\rho \Lambda n_z \rangle. \quad (48)$$

The transformation of the matrix elements (48) from cylindrical to Cartesian coordinates requires the overlaps:  $\langle n_x n_y n_z | n_\rho \Lambda n_z \rangle$ . We use the formulas given in [54]. Let us recall:

$$\begin{aligned} \langle n_x n_y n_z | n_\rho \Lambda n_z \rangle &= \delta_{2n_\rho + \Lambda, n_x + n_y} (-i)^{n_y} (-1)^\Lambda \left[ \frac{n_x! n_y! n_z! (n_\rho + \Lambda)!}{2^{2n_\rho + \Lambda}} \right]^{1/2} \\ &\quad \times \sum_{p=p_{\min}}^{p_{\max}} \frac{(-1)^p}{p! (n_x - p)! (p + n_\rho - n_x)! (n_\rho + \Lambda - p)!}, \end{aligned} \quad (49)$$

with:

$$p_{\min} = \begin{cases} 0 & \text{for } n_\rho \geq n_x, \\ n_x - n_\rho & \text{for } n_\rho \leq n_x, \end{cases} \quad (50)$$

and:

$$p_{\max} = \begin{cases} n_x & \text{for } n_x \leq n_\rho + \Lambda, \\ n_\rho + \Lambda & \text{for } n_x \geq n_\rho + \Lambda. \end{cases} \quad (51)$$

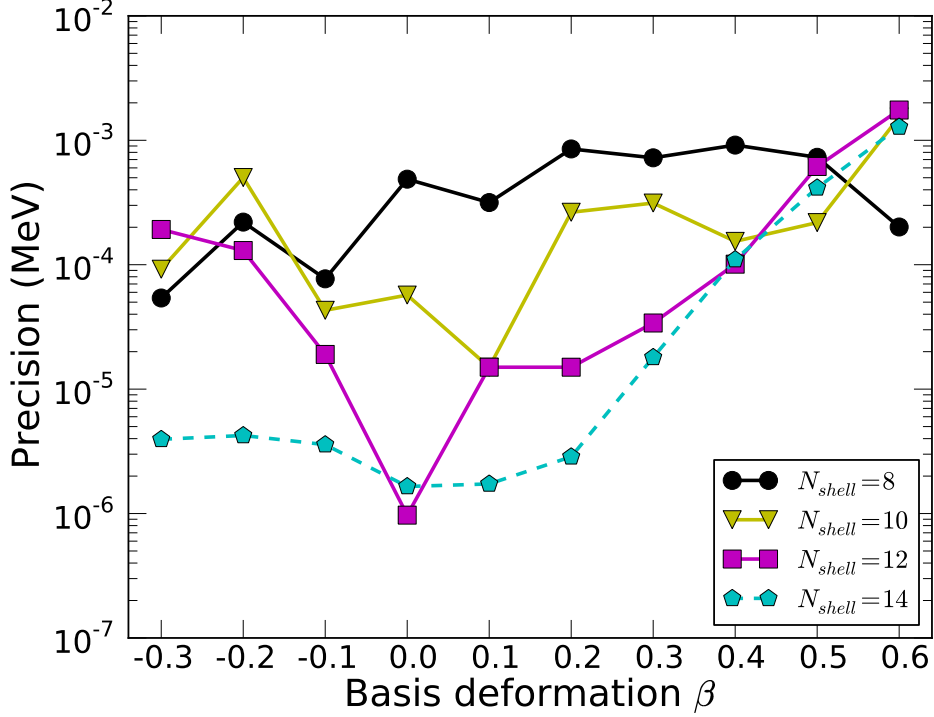


Figure 5: Stability of the HFODD solution after restart from HFBTHO at the spherical point in  $^{152}\text{Dy}$ , as function of the deformation  $\beta_2$  of the HO basis.

The overlaps for  $\Lambda < 0$  are obtained from those with  $\Lambda > 0$  according to:

$$\langle n_x n_y n_z | n_\rho \Lambda_{(<0)} n_z \rangle = (-1)^{|\Lambda|} \langle n_x n_y n_z | n_\rho \Lambda_{(>0)} n_z \rangle^*. \quad (52)$$

**Phase transformation** - After the matrices  $\mathcal{H}^{(\sigma\sigma')}$  are obtained in Cartesian coordinates, the phase transformation, Eqs. (78a)-(78b) of Ref. [1], is performed. Let us recall that it reads:

$$\begin{aligned} |n_x n_y n_z, s = +i\rangle &= \frac{1}{\sqrt{2}} \left( i^{n_y} |n_x n_y n_z, \sigma = \frac{1}{2}\rangle - i^{-n_y+1} |n_x n_y n_z, \sigma = -\frac{1}{2}\rangle \right), \\ |n_x n_y n_z, s = -i\rangle &= \frac{1}{\sqrt{2}} \left( -i^{n_y+1} |n_x n_y n_z, \sigma = \frac{1}{2}\rangle + i^{-n_y} |n_x n_y n_z, \sigma = -\frac{1}{2}\rangle \right), \end{aligned} \quad (53)$$

where  $s = \pm i$  is the y-simplex. In HFBTHO, simplex and time-reversal symmetries are always conserved (by construction), so that the HFB matrix is block diagonal:  $\mathcal{H}^{(ss')} = \delta_{ss'} \mathcal{H}^{(s)}$  and  $\mathcal{H}^{(-s)} = \mathcal{H}^{(s)*}$ . The blocks  $\mathcal{H}^{(s=\pm i)}$  are obtained by linear combinations of the  $\mathcal{H}^{(\sigma\sigma')}$  and the phase factors recalled in Eq.(53).

For axially- and parity-symmetric HFB solutions, the interface between HFBTHO and HFODD gives a precision at restart that ranges from 1 eV to 1 keV depending on the nucleus, the characteristics of the basis and the quadrupole deformation of the solution. Almost all the error is contained in the direct Coulomb energy which is computed differently in the two codes. Figure 5 shows the stability of the HFODD iterations immediately after restart from the HFBTHO solution at the spherical point in  $^{152}\text{Dy}$ , for different deformations of the basis and different basis sizes.

### 2.2.5 Mixing of Matrix Elements of the HFB Matrix

When solved by successive diagonalizations, as in HFODD, the Hartree-Fock equations are self-consistent. In practice, the iterative scheme is started with a set of initial conditions, formally some vector  $\mathbf{V}^{(0)}$ , that linearize the problem. Upon entering iteration  $m$  with a vector  $\mathbf{V}_{\text{in}}^{(m)}$ , solving the HF equations yields a new vector  $\mathbf{V}_{\text{out}}^{(m)}$ . This vector is then used as input to the next iteration  $m + 1$ ,  $\mathbf{V}_{\text{in}}^{(m+1)} \rightarrow \mathbf{V}_{\text{out}}^{(m)}$ . The iterations stop when  $|\mathbf{V}_{\text{out}}^{(m+1)} - \mathbf{V}_{\text{out}}^{(m)}| \leq \varepsilon$ , with  $\varepsilon$  a measure of the convergence. In practice, the input vector at iteration  $m + 1$  must be a mixing of  $\mathbf{V}_{\text{in}}^{(m)}$  and  $\mathbf{V}_{\text{out}}^{(m)}$  for the iterations to converge. This mixing can be a simple linear mixing of the type:

$$\mathbf{V}_{\text{in}}^{(m+1)} = \alpha \mathbf{V}_{\text{out}}^{(m)} + (1 - \alpha) \mathbf{V}_{\text{in}}^{(m)} \quad (54)$$

or more elaborate such as produced by the Broyden method [55].

Both the linear and Broyden mixing are implemented in HFODD. By default, the iterated quantities  $\mathbf{V}$  are the values of the HF fields on the Gauss-Hermite integration mesh [6]. However, it was noticed that when the Lipkin-Nogami (LN) prescription is used, the matrix elements of the density matrix in the HO basis must also be added in order to ensure convergence. In the simplest case where time-reversal and simplex symmetries are conserved, and the LN procedure is applied to both protons and neutrons, the size of the Broyden vector is augmented by  $4M^2$ , where  $M$  is the size of the s.p. basis. For large bases, the size of the Broyden vector can thus become prohibitive. To by-pass this memory bottleneck, the mixing of the matrix elements of the HFB matrix has been implemented.

In HFODD, the self-consistent loop is organized in such a way that at each iteration  $m$ , it is initialized with the set of HF fields (for neutrons and protons)  $\mathbf{V}_{\text{in}}^{(m)}$ , and ends with the determination of the new fields  $\mathbf{V}_{\text{out}}^{(m)}$ : it therefore lends itself naturally to mixing the HF fields. By contrast, the mixing of the matrix elements of the HFB matrix is most easily performed when the self-consistent loop starts with an initial HFB matrix  $\mathbf{H}_{\text{in}}^{(m)}$  and ends with the computation of the new HFB matrix  $\mathbf{H}_{\text{out}}^{(m)}$  (this is the case, e.g., in HFBTHO). In order to conserve the 'HF potential-oriented' structure of the self-consistent loop of HFODD, the mixing of the matrix elements of the HFB matrix must be done immediately after a new  $\mathbf{H}_{\text{out}}^{(m)}$  has been calculated: in HFODD such a condition actually requires independent mixing for protons and neutrons with two separate calls to the mixing routine and, in the case of the Broyden mixing, two different memory arrays.

The size of the Broyden vector (for one isospin only) depends on the symmetries of the problem: simplex conserved ISIMPY=1 or broken ISIMPY=0, time-reversal symmetry conserved IROTAT=0 or broken IROTAT=1, HFB calculations IPA HFB=1 or HF calculations IPA HFB=0. Taking also into account the symmetries of the matrix of the mean field and pairing field, the size of the Broyden vector is:

$$N = (1 + \text{IROTAT}) \times M^2 + (1 - \text{ISIMPY}) \times M^2 \\ + \text{IPA HFB} [M(M + 1)/2 + \text{IROTAT} \times M(M - 1)/2] \quad (55)$$

For a typical static HFB calculation with conserved time-reversal and simplex symmetry, a stretched basis such that NXHERM=NYHERM=30, NXHERM=60 and  $M = 1000$ , and 7 iterations conserved in memory, the Broyden method requires 302 MB of RAM when fields are mixed, and about 168 MB when matrix elements are mixed.

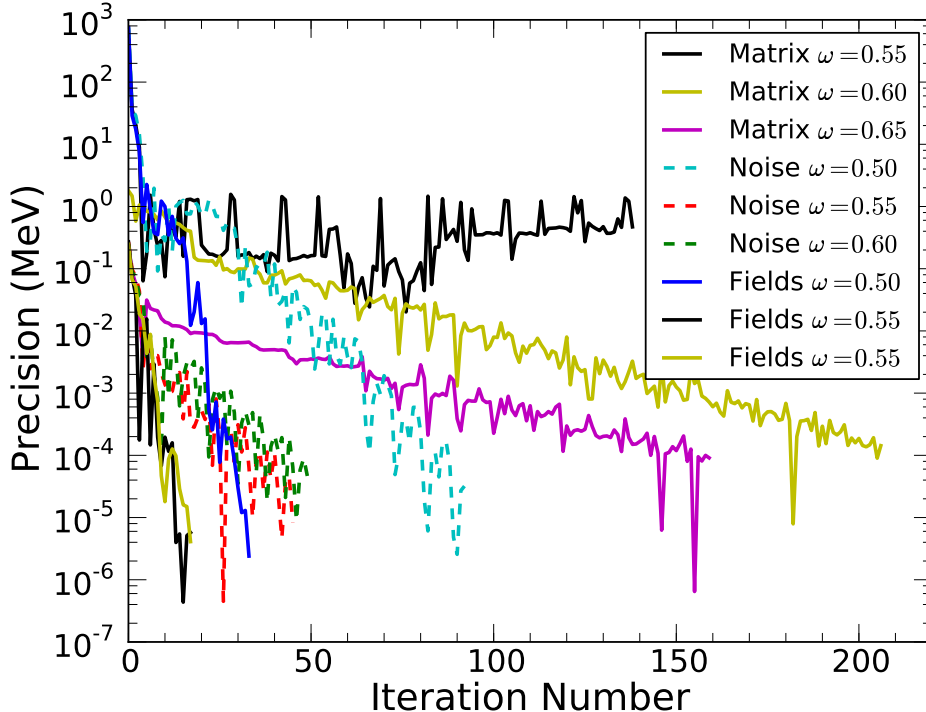


Figure 6: Convergence of the Cranking HF iterations in  $^{151}\text{Tb}$  with the Broyden method. Curves labeled 'Matrix' correspond to the original mixing of matrix elements; curves marked 'Noise' to the mixing of matrix elements when the Broyden memory is erased every 4 iterations; curves marked 'Fields' correspond to the mixing of HF fields on the Gauss-Hermite mesh.

It has been observed that the mixing of the matrix elements of the HFB matrix in HFODD is less stable than in a comparable implementation in HFBTHO. This numerical noise may be due to the fact that HFODD breaks a number of symmetries that are conserved in HFBTHO, and which manifest themselves by numerically small, non-zero elements in the matrix. Correct performance for ground-state calculations can still be obtained if the memory of the Broyden method is erased every  $n$  iterations, with  $n < n_{\text{mem}}$  where  $n_{\text{mem}}$  is the number of iterations retained to compute the full Broyden correction (noise cancellation). In practice  $n_{\text{mem}} = 4$  gives decent results.

## 2.3 Parallel Programming Model

Starting in version (v2.49t), the code HFODD has built-in parallel capabilities. These capabilities are controlled by 3 different pre-processor options and are discussed below.

### 2.3.1 Distributed Memory Parallelism

Density functional theory is an efficient method to compute the properties of multi-fermionic systems. From a programming point of view, recasting all degrees of freedom of the problem into a single function of  $\mathbf{r}$ , the local one-body density matrix, allows the formulation of a

compact, CPU- and memory-thrifty, implementation. In practice, the average computation time of standard nuclear EDF solvers ranges from a few seconds for a spherical closed-shell nucleus up to a few hours for a full symmetry-breaking configuration in a heavy nucleus.

Such naive estimates, however, are deceptive: in many instances, the nature of the problem at hand requires the computation of *many* such configurations, as for example in the determination of Potential Energy Surfaces (PES), which are critical ingredients in the proper description of the nuclear fission process. While the time of calculation of any point of the N-dimensional PES may be of the order of a few hours, systematic and accurate mapping of the surface is required to compute reliable estimates of barrier heights, tunneling probabilities or collective inertia. For  $N = 5$  degrees of freedom with  $n_i = 10$  sample points each, the size of the mesh is 100,000: such a problem requires both supercomputers and an adapted programming model.

One giant simplification of high-performance computing applications with EDF methods is that the theory generates by construction a naturally parallel computational problem: most of the time, all configurations can be handled independently by a single core (CPU unit) of a multi-core processor. The amount of inter-processor communication is therefore often rather low (coarse granularity). Such a property has made it possible to compute the entire mass table in less than a day [51].

The distributed memory programming model of HFODD contains two layers of parallelism managed by the standard Message Passing Interface (MPI) library. The outermost layer corresponds to  $N_{\text{master}}$  master groups of cores, each group being in charge of computing a given nuclear configuration. The innermost or group layer is made of the  $N_{\text{proc}}$  cores in any given group. The division of the processor grid in these two layers is carried out at the very beginning of the code using standard MPI group and communicator routines. Most applications of HFODD do not require the group structure, that is,  $N_{\text{proc}} = 1$  is sufficient most of the time. Examples of distributed HFB calculations are discussed in Sec. 2.3.4.

From a user's point of view, running HFODD on several cores requires the following:

- The code must be compiled by setting the pre-processor option `USE_MPI=1`. The user is in charge of ensuring that an implementation of MPI exists on his/her system.
- Input data now falls into 2 categories: process-dependent and process-independent data, the word 'process' referring to a given HFB calculation. Process-independent data is everything that will be the same on every process. Contrariwise, process-dependent data is what changes from one process to the next: it is therefore what distinguishes the nuclear configurations ( $Z$ ,  $N$ , constraints, etc.). For practical reasons, see Section 2.3.2, process-independent data will *always* be contained in the file `hfodd.d`, and the process-dependent data *always* in the file `hfodd_mpiio.d`.

### 2.3.2 Scalable Input Routines

In its single core version, HFODD reads its input data from the system standard input. In practice, data is often contained in a simple ASCII text file, and the execution of the code uses input redirection. Input is read by the routine `NAMALI`, which loops over the file for specific keywords, each keyword being immediately followed by the relevant data. Such a structure provides good flexibility, since the user can add or remove keywords at will from the input file.

In parallel mode, duplicating this structure of the I/O operations on all available cores is not efficient, and can in fact affect the stability of the entire system. Indeed, not only would all cores try to access the disks more or less at the same time, but they would all access the *same* file and seek different positions in it. It is a well-known rule of thumb that parallel I/O has to be handled either by one core only, or using dedicated libraries. In the specific case of HFODD, the amount of input data is rather small, common to and needed by all cores, and read only at the beginning of the calculation. The most natural solution is therefore to assign one core to the task of reading it and broadcasting it to the others.

However, the flexibility induced by the keyword structure of the input file now becomes a disadvantage, since the amount of data to be read (and then broadcast) is in fact known only at run time. This feature suggests the use of Fortran 90 linked lists for each basic type of input data (integer, double precision real number and character string). The entire I/O operation is then broken down in 3 phases: (i) construction of the linked list (ii) broadcast and (iii) reconstruction of local data. In the first phase, the routine `mpi_getSequentialData()` parses the file `hfodd.d`, which has exactly the same structure as the standard HFODD input file, and for each data, adds a node to the relevant linked list. At the end of the process, linked lists are copied to local allocatable arrays which are then broadcast to all cores using the MPI routine `MPI_Bcast` (second phase). All cores then acquire a local (to a given core) copy of 3 arrays, for the 3 basic types of data mentioned above. Finally, every element of these arrays is re-associated with the relevant local HFODD variables (third phase). This is done by the routine `mpi_setSequentialData`.

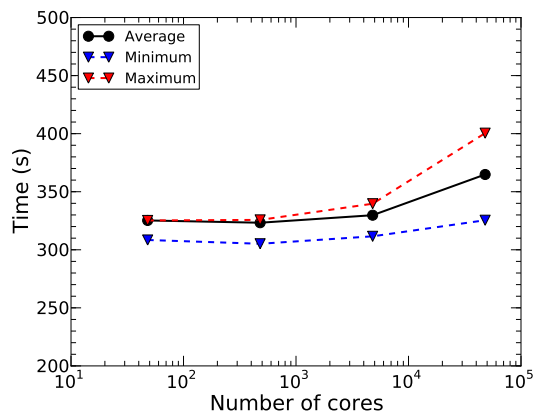


Figure 7: Average, minimum and maximum CPU time for 6 HFB iterations in  $^{152}\text{Dy}$  as a function of the number of cores for a full spherical HO basis of  $N_{\text{shell}} = 14$  shells. The pairing cut-off energy is  $E_{\text{cut}} = 60$  MeV. Calculations were done on the Cray XT5 at NCCS, the code was compiled with the PGI v.10.3 compiler with `-fast -Mipa=fast` options. The Cray `libsci` library was used for BLAS and LAPACK. All cores do the same HFB calculation.

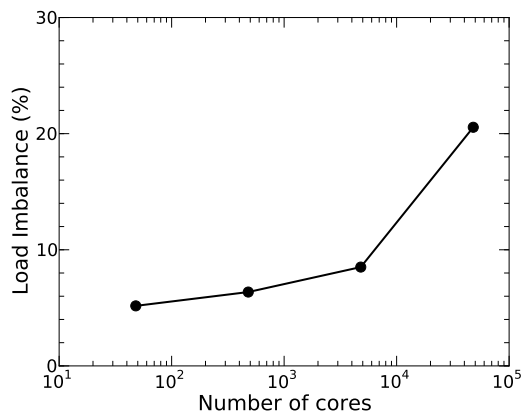


Figure 8: Load imbalance for the same runs as in Fig. 7. Load imbalance is defined here as  $(T_{\text{max}} - T_{\text{min}})/T_{\text{avr}}$ , where  $T_{\text{min}}$  (resp.  $T_{\text{max}}$ ) is the minimum (resp. maximum) time of execution over all cores, and  $T_{\text{avr}}$  the average time over all cores.

In principle, it would have been enough to implement this scheme for the standard HFODD

input file, and add a few keywords relevant for process-dependent data. However, it proved more convenient to put all process-dependent data in a file of its own, with a similar keyword structure. The I/O process described above has therefore to be repeated for the process-dependent data. This is carried out by the routines `mpi_getParallelData()` and `mpi_setParallelData`.

This implementation of the I/O procedure combines a number of advantages. First and paramount, it scales well with the number of cores available, since only one core is dedicated to accessing the disk and reading the data. Since the amount of data will always be very small (a few kB at most), the broadcast phase should not induce a very large communication overhead. In addition, the linked list structure conserves the flexibility to add/remove data from the input files, which also ensures backward and forward compatibility with all future releases of the code.

Figure 7 shows the scaling properties of HFODD. The sample calculation consisted of 6 HFB iterations in  $^{152}\text{Dy}$  in a full spherical basis of  $N = 14$  shells with constraints on  $Q_{20} = 20$  b and  $Q_{22} = 0$  b. All cores computed the same configuration. The PGI compiler v10.3 with the `-fast -Mipa=fast` options was used to compile the code, the Cray library `libsci` to link to BLAS and LAPACK, and all calculations were done on the Jaguar Cray XT5 at the NCCS. These technical characteristics are given because the actual time of execution can vary very significantly depending on the compiler/platform and compiler options used.

Since all cores perform exactly the same calculation, any departure from a flat straight line should be attributed at first order to (i) the inter-core communication during the initial input setup (ii) filesystem operations to create/access files. While the input setup has been somewhat optimized, see above, all other I/O operations are the same as in serial mode: for the runs shown in Figs. (7-8), every core generates 2 files that remain opened with read/write permissions for the entire time of execution. To better grasp the impact of the lack of I/O optimization, figure 8 shows the load-imbalance of this calculation, defined here as:

$$\text{LI} = \frac{T_{\max} - T_{\min}}{T_{\text{avr}}} \quad (56)$$

where  $T_{\min}$  (resp.  $T_{\max}$ ) is the minimum (resp. maximum) time of execution over all cores, and  $T_{\text{avr}}$  the average time over all cores. Perfect load-balancing (equal distribution of work between cores) implies  $\text{LI}=0$ .

### 2.3.3 Shared Memory Parallelism

Many leadership class computers have adopted a hybrid distributed-shared memory architecture, whereby all cores are grouped into processors, each processor having access to its own physical memory. Tests of the current version of HFODD have been carried out on the Franklin Cray XT4 and Jaguar Cray XT5, which are characterized by, respectively, 4-core processors with 8 GB shared memory and 12-core processors with 24 GB shared memory. As mentioned earlier, most applications of HFODD can run on a single core, so that in the case of the Jaguar supercomputer, 12 simultaneous calculations can be run on a processor. However, for large basis size, the memory needed by one instance of HFODD can exceed the 2 GB/core available.

This seemingly limitation of the prevailing architectures can be exploited to accelerate the execution of the code by using the standard OpenMP API. If the number of instances of the code running on a given processor is less than the actual number of cores in that processor, several cores are in fact inactive. The OpenMP API offers a very simple interface to recycle these cores

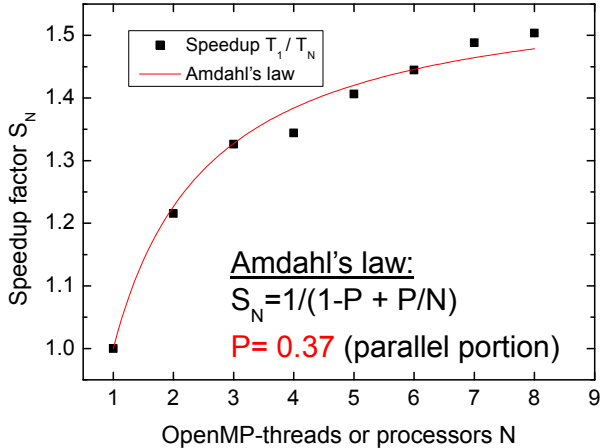


Figure 9: Multi-threading accelerations in HFB calculations of  $^{180}\text{Hg}$  for a deformed  $N_{\text{shell}} = 26$  HO basis with 1140 states and deformation  $\alpha_{20} = -0.32$ . Calculations were performed on a Intel Xeon processor with the Intel Fortran Compiler and the `-xSSE4.2 -O3 -override-limits` options with standard BLAS libraries, and are compared to Amdahl’s law.

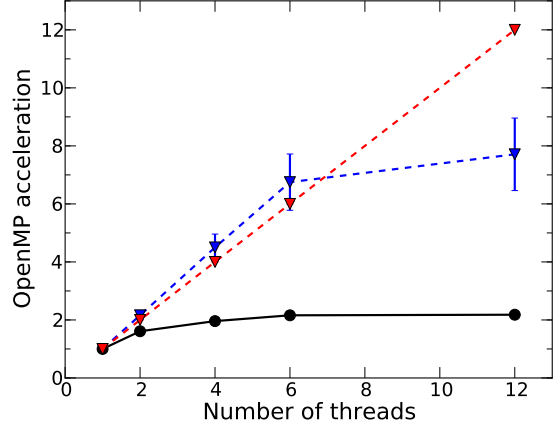


Figure 10: Same as Fig. 9 for 6 HFB iterations in  $^{152}\text{Dy}$  in a full spherical basis of  $N = 14$  shells (same characteristics as in Fig. 7) and threaded BLAS libraries. Black circles: speed-up of the entire code; triangles: speed-up for the 3 impacted routines (error bars reflect the rounding of the time to the nearest second). Dashed line: perfect scaling for the OpenMP acceleration.

for quasi-automatic parallelization of the code (multi-threading). The execution then consists of series of sequential instructions (on one core) combined with multi-core parallel sequences. This mechanism is particularly effective to (quasi-)automatically parallelize loops. Let us recall that OpenMP instructions, or pragmas, are coded in the form of comments only activated by the relevant option of the compiler: modifications of the source code remain minimal.

We identified 3 subroutines of HFODD that could take a significant chunk of the total run time: subroutine DENMAC computes the density matrix from the HFB eigenvectors; subroutine SPAVER computes s.p. expectation values of operators; subroutine NILABS defines the Nilsson labels of s.p. states. All these routines involve 3-nested loops with  $N_{\text{states}}$  elements, where  $N_{\text{states}}$  is the number of basis states. For large bases with  $N_{\text{states}} \approx 1000 - 2000$ , these loops become time-consuming, and they cannot be re-arranged easily in a way that memory access is optimized.

Figure 9 shows the OpenMP acceleration of a full HFB calculation in  $^{180}\text{Hg}$  with a large basis of 26 HO shells and 1140 states (basis deformation  $\alpha_{20} = -0.32$ ) as function of the number of threads. Calculations were performed on a cluster of Intel Xeon processors with the Intel Fortran Compiler and the `-xSSE4.2 -O3 -override-limits` options. Standard (un-threaded) BLAS and LAPACK libraries were used. The 3 routines impacted by Open MP pragmas represent a small fraction  $P = 0.37$  of the total execution time in this case, and the observed acceleration nicely aligns with predictions by the empirical Amdahl’s model.

Leadership class computers often provide threaded BLAS libraries. In Fig. 10, we shows the acceleration induced by OpenMP in the same test case as in Sec. 2.3.2. This profiling

experiment was done on the Jaguar Cray XT5 computer at the NCCS by linking to threaded BLAS libraries. At the level of the 3 modified routines, the scaling is perfect with the number of threads; overall acceleration is a little better than in the case of Fig. 9 due to the benefit of using threaded libraries. OpenMP acceleration is activated by setting `USE_OPENMP` to 1 in the Makefile.

### 2.3.4 Parallelization of Diagonalization Routines

One strength of the HFODD code is its ability to perform computations without assuming symmetries. Calculations without symmetries, however, prove computationally expensive. Until now HFODD has been successfully used in several massively parallel applications, such as the survey of one quasi-particle states in odd mass nuclei [53] and potential energy surfaces for fission [56]. The trend in massively parallel computing, however, is to reduce the memory available to each computing core, thereby indirectly imposing restrictions on the symmetries assumed in current-generation HFODD calculations. In Fig. 11, the peak memory used in a HFODD run is plotted against the number of full shells in the harmonic oscillator basis. It is worth noting that the present NCCS Cray XT4 and Cray XT5 machines have 2GB available to a core, which is exceeded by a problem using 20 full oscillator shells. For problems like fission that require the calculation of highly deformed nuclei, at least 26 – 31 oscillator shells can be needed.

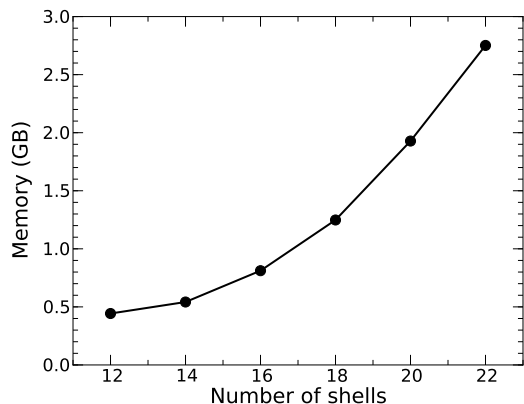


Figure 11: The memory high-water mark attained by HFODD is plotted against the number of major harmonic oscillator shells used in the basis.

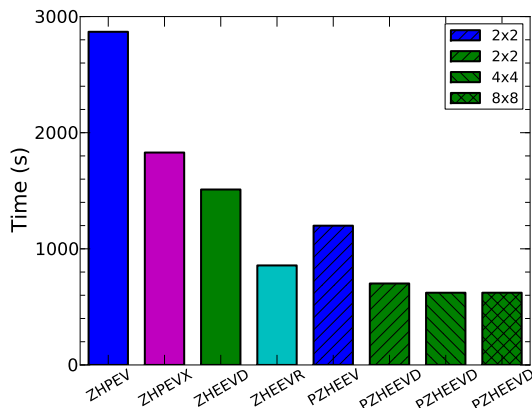


Figure 12: Total execution time of HFODD spent for different diagonalization routines and numbers of rows used in a square ScaLAPACK process grid. For single-core tests, HFBISZ was modified so that all eigenstates of the HFB matrix are computed, to allow meaningful comparisons with multi-core algorithms.

To fully take advantage of the next generation of massively parallel platforms as well as its full symmetry-breaking capabilities, HFODD should therefore be scaled so that its solution of the HFB equations is distributed among an arbitrary number of cores. Before undertaking such a daunting task, though, the anticipated benefits must be assessed and demonstrated. In

this release of the code, we have tested whether we can achieve any gain in the speed of the diagonalization routines by using the ScaLAPACK library.

Tests were conducted for the all symmetry-breaking HFB case (subroutine HFBSIZ), which involves the largest matrices, of size  $4N \times 4N$  if  $N$  is the number of states in the HO basis. Fig. 12 shows the time of execution of 3 HFB iterations in  $^{152}\text{Dy}$  in a full spherical HO basis of  $N_{\text{shell}} = 14$  shells ( $N = 680$  states). The code was compiled with the `-fast -Mipa=fast` option and run on the Cray XT5 computer at the NCCS. OpenMP acceleration was activated, and the BLAS and LAPACK routines were provided by the `libsci` library. Fig. 12 shows the benchmark results for different diagonalization methods and different ScaLAPACK core grids. Let us note that the ScaLAPACK library does not include a parallelized version of all LAPACK diagonalization routines. From the strict perspective of execution time, the single-core version of HFODD invoking the ZHEEVR LAPACK routine (based on a very fast diagonalization algorithm) may turn out to be faster than the multi-core version, which can only resort to PZHEEV or PZHEEVD ScaLAPACK methods.

The module `hfodd_sl` provides an interface to the parallel matrix diagonalization routines available in ScaLAPACK. The user may enable the use of the `hfodd_sl` module by setting the environment variable `USE_SCALAPACK` to 1 in the project Makefile (similarly, `USE_SCALAPACK` is set to 0 to disable the module). The `hfodd_sl` module requires that the program is linked to a ScaLAPACK library and compiled with MPI, as well. The user should also specify the size of the process grid in the project Makefile through the environment variables `M_GRID` (number of process rows) and `N_GRID` (number of process columns). The program will stop with an error, if the product `M_GRID`  $\times$  `N_GRID` times the number of different HFB configurations exceeds the number of processes allocated for the program.

## 2.4 Corrected errors

In the present version (v2.49t), we have corrected the following little significant errors of the previous published version (v2.40h) [6].

### 2.4.1 Coulomb energies

For the combination of the Coulomb parameters `ICOUDI=1` and `ICOUEX=2` (`ICOUDI=2` and `ICOUEX=1`), the direct (exchange) Coulomb energy was inadvertently set to zero.

### 2.4.2 Skyrme parameters

For SLY5 and SLY7, the predefined values of the Skyrme-force parameters corresponded to those given in Ref. [57], while for SLY4 they corresponded to unrounded numbers communicated by the authors of the force. At present, all these parameters are coded according to Ref. [58], while the previous values are kept in the code under acronyms `sLy4`, `sLy5`, and `sLy7`.

### 2.4.3 Quasiparticle blocking

The time reversal of s.p. states was incorrectly coded for `IDSIGB = -1` (in `BLOSIG`), `IDSIMB = -1` (in `BLOSIM`) `IDSIQB = -1` (in `BLOSIQ`), `IDSIZB = -1` (in `BLOSIZ`). Moreover, the quasiparticle blocking was incorrectly performed in `BLOSIZ` and, in some situations, these errors compensated

one another. One should stress that the calculated results were always correctly converged, but they could have corresponded to other blocked quasiparticles as compared to what was requested in the input data.

#### 2.4.4 Yukawa mean fields

For calculations related to the Yukawa interaction that were not supposed to be using the mean fields stored on the disc (IFCONT = 0), in the first iteration the Yukawa mean fields were inadvertently set to zero. Since later these mean fields were calculated correctly, the error was only affecting the continuation of calculations from the disc, while the converged results were correct.

#### 2.4.5 The Broyden method

In the subroutine DOBROY, the input parameter ALPHAM was inadvertently reset to 1-SLOWEV and thus it was ineffective.

## 3 Input Data File

### 3.1 Physics

**Keyword:** PROJECTISO

0, 2, 1, 1.E-6, 0, 0 = IPRGCM, ISOSAD, NBTKNO, EPSISO, ICSKIP, IFERME  
 For  $IPRGCM \geq 1$  and  $NBTKNO \geq 1$ , the isospin projection is carried out. The isospin projection is performed for all values of isospin  $T$  such that  $T_{\min} \leq T \leq T_{\min} + \Delta T$ . In the current implementation,  $T_{\min} = (N - Z)/2$ , and  $\Delta T := ISOSAD/2$ . The number of Gauss-Legendre points required to perform integrations over the Euler angle  $\beta_T$  is given by NBTKNO. By setting ICSKIP=1, in the projection routines the Coulomb interaction can be switched off, that is, in Eq. (7)  $\hat{V}^C$  can be neglected. Parameter EPSISO gives  $\varepsilon_T$  and controls the number of good-isospin states. Parameter IFERME controls the calculation of the Fermi matrix element (13), which proceeds in two independent runs. In the first run, for IFERME=-1, the wave-function  $|I = 0, T \approx 1, T_z = \pm 1\rangle$  is computed and stored in the external file under the name specified in the keyword WAVEF-FILE. Next, for IFERME=+1, the matrix element (13) is computed. This run uses information on the  $|I = 0, T \approx 1, T_z = \pm 1\rangle$  state calculated in the first step and supplied in the file specified again in the keyword WAVEF-FILE.

Current restrictions: In version (v2.49t), the isospin projection is only available at the Hartree-Fock level, that is, it requires IPAIRI=0. When the full Hamiltonian is re-diagonalized (ICSKIP=0), the Coulomb potential must be computed exactly, that is, by expanding both the direct and exchange terms onto a sum of Gaussians, see Sec. 2.10 of Ref. [7]. This requires setting ICOUDI=2 and ICOUEX=2 in the input. The method also imposes setting IROTAT to 1. Note also that  $IPRGCM \geq 1$  activates either the isospin-, or angular-momentum projection, or both (see keyword PROJECTGCM described in [7]). To run the isospin- or angular-momentum projection alone, one needs to set the numbers of integration points NUAKNO=1 and NUBKNO=1 or NBTKNO=1, respectively.

**Keyword: COULCHARG**

$$1.0 = E\_EFFE$$

$E\_EFFE$  is the factor that multiplies the value of the elementary charge used in the Coulomb mean-field. In this way the strength of the Coulomb interaction can be modified or, for  $E\_EFFE=0$ , the Coulomb interaction can be switched off. Note that this factor does not change the strength of the Coulomb interaction rediagonalized within the isospin-projection method, see Sec. 2.1.1.

**Keyword: FINITETEMP**

$$0.0 = TEMP\_T$$

This keyword controls the value of the nuclear temperature (in MeV). If  $TEMP\_T>0$ , The finite-temperature HFB or HF+BCS calculations are performed.

**Keyword: SHELLCORCT**

$$0 = IFSHEL$$

For  $IFSHEL=1$ , the traditional shell correction  $\delta R_{\text{shell}}^{(1)}$  is computed at convergence from the HF s.p. energies. If  $IFSHEL=2$ , the shell correction  $\delta R_{\text{shell}}^{(2)}$  is computed, which includes the removal of spurious contributions from positive energy states. For  $IFSHEL=0$ , shell correction is not computed.

**Keyword: SHELLPARAM**

$$1.2, 1.2, 4.5, 6 = GSTRUN, GSTRUP, HOMFAC, NPOLYN$$

This item adjusts the parameters of the shell correction. The variable  $GSTRUN$  ( $GSTRUP$ ) stands for the  $\gamma_n$  ( $\gamma_p$ ) smoothing parameter for the neutrons (protons).  $HOMFAC$  is the multiplicative factor  $\alpha$  that defines the energy window for the shell correction, according to  $\alpha\hbar\omega$ , with  $\hbar\omega = 41/A^{1/3}$ .  $NPOLYN$  is the number  $p$  of Hermite polynomials used in the expansion of the smooth density. Preset values are a good choice to use for  $IFSHEL=1$ . For  $IFSHEL=2$ , the recommended values are  $\gamma_n = 1.54$ ,  $\gamma_p = 1.66$ ,  $\alpha = 4.5$  and  $p = 10$ .

**Keyword: RENORMASS**

$$0, 0.0, 0.0, 0.0 = IRENMA, DISTAX, DISTAY, DISTAZ$$

For  $IRENMA \geq 1$  the renormalized translational mass is determined in each iteration by using components of the shift vector  $\mathbf{R}$ ,  $DISTAX$ ,  $DISTAY$ , and  $DISTAZ$  (in fm), in the  $x$ ,  $y$ , and  $z$  direction, respectively, multiplied by  $IRENMA$ , see Eqs. (38) and (40). For  $IRENMA=0$ , the mass is not renormalized.

**Keyword: GAUOVERAPP**

$$1 = IDOGOA$$

For  $IDOGOA=0$  or 1, the translational mass is determined by using the Lipkin method (38) or the GOA expression (40), respectively. However, even for  $IDOGOA=0$  the GOA mass is calculated and printed for reference. For  $IRENMA=0$ , the value of  $IDOGOA$  is ignored.

**Keyword: UNEDF\_PROJ**

$$0 = IF\_EDF$$

Setting  $IF\_EDF=1$  activates specific parameterizations of the Skyrme energy functional for which volume coupling constants are determined automatically from nuclear matter properties (used as inputs) and surface coupling constants are preset as usual, following the strategy laid out in [59].

## 3.2 Numerical Methods

**Keyword:** TWOBASIS

0 = ITWOBA

For ITWOBA=1, the two-basis method is used to diagonalize the HFB Hamiltonian. ITWOBA=1 requires IPAHFB=1. The two-basis method is currently implemented only for the no-symmetry case; therefore, ITWOBA=1 requires ISIMPY=0 and IPARTY=0.

**Keyword:** CUT\_SPECTR

0 = LIMQUA

For LIMQUA=1, the HFB quasiparticle energies are calculated only up to the cut-off energy of ECUTOF, see Sec. 3.1 in [4]. LIMQUA=1 requires IPAHFB=1.

**Keyword:** MULTLAGRAN

0, 0, 0.0, 0 = LAMBDA, MIU, QLINEA, IFLALQ

For IFLALQ=1, the linear multipole constraint is used in conjunction with the quadratic multipole constraint (see keyword MULTCONSTR) to implement the ALM for the total multipole moment constraint of multipolarity  $\lambda$  and  $\mu$ . The value of QLINEA is the initial value for the Lagrange parameter  $L_{\lambda\mu}^{(0)}$ . Updates of the parameter in the ALM method are defined by Eq. (45). The calculated values of the Lagrange parameters are stored on the record file; this allows for a smooth continuation of the ALM method when restarting calculations from disk, see keyword CONTAUGMEN.

For IFLALQ=-1, only the linear multipole constraint is used for the multipolarity  $\lambda$  and  $\mu$ . This option is used together with IF\_RPA=1. For IFLALQ=0, linear constraints are switched off.

**Keyword:** SURFLAGRAN

0, 0, 0.0, 0 = LAMBDA, MIU, SLINEA, IFLALS

This keyword is the exact analog of MULTLAGRAN for surface and Schiff moments, see keywords SURFCONSTR or SCHICONSTR) in Sec. 2.4 of [4]. Additional values for the flag IFLALS are possible: for IFLALS=2 or 3, the ALM is applied only for the neutron or proton (surface-moment or Schiff-moment), respectively. The values of IFLALS must be the same for all constrained multipolarities.

**Keyword:** CONTAUGMEN

0 = IACONT

For IACONT=1, the Lagrange parameters  $L_{\lambda\mu}$  for the linear constraints will be initialized with the values read from the record file.

**Keyword:** RPA\_CONSTR

0 = IF\_RPA

For IF\_RPA=1, the Lagrange parameters  $L_{\lambda\mu}$  of the linear constraints will be updated automatically at each iteration based on the approximation of the RPA matrix. In HFODD version (v2.49t), this option is only available for HFB calculations for conserved simplex (ISIMPY=1). To be activated, it also requires the flags for linear constraints IFLALQ to be set (see keyword MULTLAGRAN). While in the ALM, these flags are all set to 1, in the method based on the RPA matrix they must be set to -1.

**Keyword:** HFBTHOISON

0, 0.0 = IF\_THO, CBETHO

For `IF_THO=1`, the code will automatically attempt to perform the requested calculation, first with the `HFBTHO` solver, then by automatic restart with the standard `HFODD` engine. All options specific to `HFODD` and not implemented in `HFBTHO` will simply be disregarded in this first stage. As an experimental feature, it is also possible to restart constrained calculations, in which case `CBETHO` is the value of the  $\beta_2$  deformation used to start `HFBTHO`.

**Keyword:** `BROYDENMAT`

4, 0 = `NOIINP`, `MIXMAT`

For `MIXMAT=1`, the iterations of the self-consistent method proceed by mixing the matrix elements of the `HF(B)` matrix instead of the `HF` fields. This option is compatible with both `IBROYD=1` and `IBROYD=0`. It has been noticed that the mixing of matrix elements is less stable than the mixing of the fields, unless the Broyden memory is erased every  $n$  iterations. The value of  $n$  is given by `NOIINP`, and it is recommended to take  $n$  less than the number of iterations kept in the Broyden memory.

**Keyword:** `PARA_ALL`

0, 1, 1, 1, 1 = `IPAALL`, `NUBSTA`, `NUBSTO`, `NUTSTA`, `NUTSTO`

For `IPAALL=1`, calculations of kernels for different values of the Euler angle  $\beta$  and the gauge angle  $\beta_T$  proceed in the same way as those for the  $\alpha$  and  $\gamma$  Euler angles, see keyword `PARAKERNEL` in Sec. 3.2 in [7]. This allows for performing the calculation of kernels in parallel (in different runs of the single-core version of `HFODD`), and later using the calculated kernels for the angular-momentum and isospin projection. Calculations are performed for the nodes in the Euler angle  $\beta$  from `NUBSTA` to `NUBSTO` and for those in the gauge angle  $\beta_T$  from `NUTSTA` to `NUTSTO`. Values of `NUBSTA` and `NUBSTO` must be between 1 and `NUBKNO` and must be ordered as `NUBSTA`  $\leq$  `NUBSTO`. Values of `NUTSTA` and `NUTSTO` must be between 1 and `NBTKNO` and must be ordered as `NUTSTA`  $\leq$  `NUTSTO`. `IPAALL=1` requires `IPAKER=1`.

**Keyword:** `NUMBKERNEL`

0 = `KFIKER`

For `KFIKER`  $>$  0, the automated procedure of naming the kernel files (see keyword `SAVEKERNEL` in Sec. 3.2 in [7]) is suspended and the kernels are saved in the kernel file carrying the consecutive number equal to `KFIKER`. This requires an explicit bookkeeping of the kernel-file names in the input data, but has the advantage of preventing two parallel jobs from accessing the same kernel file simultaneously. Only the values of `KFIKER` between 0 and 999 are allowed. `KFIKER`  $>$  0 requires `IPAKER=1`.

## 3.3 High-Performance Computing

### 3.3.1 List of active keywords in `hfodd.d`

In parallel mode, the code `HFODD` (v2.49t) reads all user-defined sequential data from the input file named `hfodd.d`. Since this version is the first to embed parallel capabilities, many `HFODD` options have not been implemented in parallel mode yet. Only a subset of `HFODD` keywords can therefore be activated, the list of which is given below:

- **Iterations** - `ITERATIONS`, `BROYDEN`, `SLOW_DOWN`, `SLOW_PAIR`, `SLOWLIPKIN`, `ITERAT_EPS`, `MAXANTIOSC`, `PING_PONG`, `CHAOTIC`,

- **Specific features** - FINITETEMP, SHELLCORCT, HFBTHOISON, SHELLPARAM, COULOMBPAR, SKYRME-SET, SKYRME\_STD, UNEDF\_PROJ,
- **Constraints** - OMEGAY,
- **Symmetries** - SIMPLEXY, SIGNATUREY, PARITY, ROTATION, TSIMPLEX3D,
- **Pairing** - PAIRING, HFB, CUTOFF, BCS, HFBMEANFLD, LIPKIN, PAIR\_INTER, PAIRNINTER, PAIRPINTER,
- **HO Basis** - OPTI\_GAUSS, GAUSHERMIT, BASIS\_SIZE, SURFAC\_DEF,
- **Miscellaneous** - ONE\_LINE, NILSSONLAB, REVIEW,
- **Restart options** - RESTART, CONT\_PAIRI, CONTLIPKIN, CONTFIELDS, EXECUTE.

In principle, these options provide enough flexibility to cover the majority of HFODD applications in parallel mode. The user interested in some specific option which could not be activated by one of the keywords above can still manually modify the routine PREDEF prior to compilation. This routine pre-defines all HFODD input data.

### 3.3.2 Structure of hfodd\_mpiio.d

**Keyword:** CALCULMODE

1, 0 = MPIDEF, MPIBAS

For MPIDEF=1, the code will perform a simple grid calculation of  $N_p \times N_n \times N_{\text{def}}$  points where  $N_p$  is the number of points along the  $Z$ -axis (proton number),  $N_n$  the number of points along the  $N$ -axis (neutron number), and  $N_{\text{def}}$  the total number of constraints on deformations, see keyword MULTICONST below. Requires IFCONS=1. For MPIBAS=1, the calculation grid will be given by  $N_p \times N_n \times N_{\text{def}} \times N_{\text{HO}} \times N_\beta \times N_\omega$ , where  $N_{\text{HO}}$  is the number of different oscillator shells in the basis,  $N_\beta$  the number of different deformations of the basis, and  $N_\omega$  the number of different oscillator frequencies (in MeV), see also keyword BASIS-NSHL, BASIS-DEFS and BASIS-FREQ below.

**Keyword:** CONSTR\_DEF

1 = IFCONS

For IFCONS=1, every calculation performed by the code will be constrained on the relevant values of the multipole moments.

**Keyword:** CONSTR\_LIN

1 = IFLINE

For IFLINE=1, constrained calculations in multi-core mode are performed with the RPA method of re-adjusting the linear constraints, see Sec. 2.2.3.

**Keyword:** ALL\_NUCLEI

66, 2, 1, 86, 2, 1 = IZSTRT, IZSTEP, NSTPEZ, INSTRT, INSTEP, NSTEPN

Define a vector of proton and neutron numbers

$$Z(i) = Z(0) + (i - 1)\delta Z, \quad i = 1, \dots, N_p, \quad N(j) = N(0) + (j - 1)\delta N, \quad j = 1, \dots, N_n. \quad (57)$$

Then,  $Z(0):=IZSTRT$ ,  $\delta Z:=IZSTEP$ ,  $N_p:=NSTEPZ$ ,  $N(0):=INSTRT$ ,  $\delta N:=INSTEP$ ,  $N_n:=NSTEPN$ . This defines a (rectangular) subset of nuclei in the isotopic chart for which (possibly  $N_{\text{def}} > 1$ ) calculations will be performed.

**Keyword:** MULTICONST

2, 0, 10.0, 10.0, 4 = LAMBDA MIU, QBEGIN, QFIN, NUMBERQ

The deformation grid is defined as a set of  $N_{\text{def}} = \prod_{\lambda\mu} N_{\lambda\mu}$  deformation points where  $N_{\lambda\mu}$  is the number of points for the constraint on the multipole moment  $\hat{Q}_{\lambda\mu}$  with multipolarity  $\lambda$  (LAMBDA) and  $\mu$  (MIU). The point number  $k$  for this constraint reads:

$$\bar{Q}_{\lambda\mu}(k) = \bar{Q}_{\lambda\mu}(0) + \frac{k-1}{N_{\lambda\mu}-1} [\bar{Q}_{\lambda\mu}(N_{\lambda\mu}) - \bar{Q}_{\lambda\mu}(0)], \quad (58)$$

with  $\bar{Q}_{\lambda\mu}(0):=QBEGIN$ ,  $\bar{Q}_{\lambda\mu}(N_{\lambda\mu}):=QFIN$  and  $N_{\lambda\mu}:=NUMBERQ$ . Multiple constraints are obtained by adding several lines with different  $\lambda$  and  $\mu$ . All such lines must begin with  $\lambda < 0$  except the last one.

**Keyword:** BASIS-NSHL

8, 2, 1 = N\_MINI, N\_STEP, NOFSHL

For MPIBAS=1, the number of shells in the basis  $N_{\text{HO}}$  can take different values of the form:

$$N_{\text{shell}}(m) = N_{\text{shell}}(0) + (m-1)\delta N_{\text{shell}}, \quad m = 1, \dots, N_{\text{HO}}. \quad (59)$$

Then,  $N_{\text{shell}}(0):=N\_MINI$ ,  $\delta N_{\text{shell}}:=N\_STEP$ ,  $N_{\text{HO}}:=NOFSHL$ . Note that the number of states is set independently as a sequential data under keyword BASIS\_SIZE. While the familiar relation  $N_{\text{states}} = (N_{\text{shell}} + 1)(N_{\text{shell}} + 2)(N_{\text{shell}} + 3)/6$  between the number of states and the number of HO shells is valid for spherical bases, it does not apply in the deformed case.

**Keyword:** BASIS-DEFS

0.0, 0.1, 1 = B20MIN, B20STP, NOFB20

For MPIBAS=1, the axial quadrupole deformation  $\beta \equiv \alpha_{20}$  can take different values of the form:

$$\beta(n) = \beta(0) + (n-1)\delta\beta, \quad n = 1, \dots, N_{\beta}. \quad (60)$$

Then,  $\beta(0):=B20MIN$ ,  $\delta\beta:=B20STP$ ,  $N_{\beta}:=NOFB20$

**Keyword:** BASIS-FREQ

8.0, 0.1, 1 = O\_MINI, O\_STEP, NOFFRE

For MPIBAS=1, the oscillator frequency  $\hbar\omega$  can take different values of the form:

$$\hbar\omega(l) = \hbar\omega(0) + (l-1)\delta\omega, \quad l = 1, \dots, N_{\omega}. \quad (61)$$

Then,  $\hbar\omega(0):=O\_MINI$ ,  $\delta\omega:=O\_STEP$ ,  $N_{\omega}:=NOFFRE$

## 4 Output Files

Four additional examples of output file, illustrating the new features of the code are provided in files ca40\_iso.out, cr48\_lip.out, cr50\_tem.out and pb208\_tho.out. Selected lines from

ca40\_iso.out are given in Appendix B below. Several minor sections of the output have been added or reformatted. We describe below only the non-trivial important additions.

In ca40\_iso.out, the section labeled ISOSPIN-MIXED EIGENSTATES lists all the eigenvectors (within the  $\epsilon_T$  cut-off described in Sec. 2.1.1) of the Hamiltonian re-diagonalized in the good-isospin basis. The first two columns are the number  $n$  and value  $E_{n,T_z}$  of the energy. The next 5 columns give the characteristics of the expansion of Eq.(12) (or Eq.(18) if isospin and angular momentum are combined). The fourth and fifth columns give respectively the number  $m$  and isospin  $T$  of the good-isospin basis state. The columns 6, 7 and 8 give, respectively, the norm of the expansion coefficient  $a_{mT}^{(n)}$ , its real part and its imaginary part.

In cr50\_tem.out, the new value I.LINE=3 has been used to display the iterations. Every line is made of the iteration number ITER, the value of the total energy ENERGY, the value of the stability criterion STABILITY, the total quadrupole moment Q\_2 the  $\gamma$  angle GAMMA, the total entropy S, the neutron Fermi level lam\_n, the proton Fermi level lam\_p, the neutron pairing energy EpN and the proton pairing energy EpP. With the values of the Fermi levels, total entropy and temperature, the grand canonical potential  $\Omega$  of Eq.(19) can be deduced at each iteration.

In pb208\_tho.out, a warning message is displayed at the beginning to indicate that the calculation will proceed in two steps, first with HFBTHO then with HFODD. The message also gives the conditions under which the restart is expected to be smooth. Follows the output generated by HFBTHO, we refer to [50] for additional information. Since the UNEDF functional is used in this test run, an additional section NUCLEAR MATTER PROPERTIES lists the volume nuclear matter characteristics of the functional. Section THE SHELL CORRECTION... gives the type of shell correction computed and the numerical characteristics of the smoothing procedure. Section SHELL CORRECTION located just before the final energy table gives the value of the shell correction for neutrons and protons.

## 5 Fortran Source Files

The Fortran source code is provided as a set of 8 module files:

- hf249t.f - Main source code
- hfodd\_functional.f90 - Definition of energy functionals based on nuclear matter properties and coupling constants instead of (t,x) parameters.
- hfodd\_shell.f - Shell correction
- hfodd\_hfbtho.f90 - HFBTHO code (v.101a)
- hfodd\_interface.f90 - Interface between HFBTHO and HFODD
- hfodd\_mpiio.f90 - Module handling I/O in parallel mode
- hfodd\_mpimanager.f90 - Module defining parallel jobs
- hfodd\_SLsiz.f90 - Scalapack module for routine HFBSIZ

together with one header file, hfodd\_sizes.h, which contains all Fortran PARAMETER statements controlling the size of static arrays. The language of newly-developed modules is Fortran 90, while legacy code is still written, in part or totally, in Fortran 77.

## 5.1 Standard Libraries

The code HFODD requires an implementation of the BLAS and LAPACK libraries to function correctly, see Sec. 5.2 in [7] for details. While the interface to older NAGLIB routines remains available, BLAS and LAPACK will give the best peak performance on most current computers and are recommended.

## 5.2 Parallel Mode

We recall that a parallel machine is made of a certain number of sockets, each containing one processor. Every processor contains a number of CPU units, or cores, sharing the same memory.

### 5.2.1 Basic MPI

To activate multi-core calculations, HFODD requires an implementation of the Message Passing Interface (MPI). The current version was tested on two different implementations:

- MPICH-1 and MPICH-2, available at:  
<http://www.mcs.anl.gov/research/projects/mpich2/>
- Open MPI available at: <http://www.open-mpi.org/>

In parallel mode, the code HFODD is compiled by setting `USE_MPI` to 1 in the project Makefile. Typically, the executable is run as follows (`bash` syntax):

```
mpiexec -np [number of processes] hf249t < /dev/null >& hf249t.out
```

where `hf249t.out` is a redirection for the standard output and files `hfodd.d` and `hfodd_mpiio.d` must be in the directory where this command is run.

### 5.2.2 Hybrid OpenMP/MPI Mode

Multi-threading is activated by switching the `USE_OPENMP` to 1 in the project Makefile. This option can be used on its own, or in combination with `USE_MPI=1`, in which case the programming model is hybrid MPI/OpenMP. We recall that to activate multi-threading, the environment variable `OMP_NUM_THREADS` must be set to the required number of threads prior to execution. If every processor has 6 cores, then to run 12 MPI processes with 3 threads each, the following command line (in the OPENMPI implementation) should be executed:

```
export OMP_NUM_THREADS = 3
```

```
mpiexec -np 12 -npersocket 2 hf249t < /dev/null >& hf249t.out
```

Therefore, instead of the 12 MPI processes being executed by all the 12 cores of 2 full processors, the `-npersocket 2` option imposes that only 2 cores within a given socket are actually used, leaving the remaining 4 available when multi-threading kicks in. Such an instruction requires 6 processors instead of 2 in the pure MPI mode, and up to  $(12 \text{ processes}) \times (3 \text{ threads}) = 36$  cores may be active at a given time .

### 5.2.3 Scalapack

Using Scalapack requires the most advanced partitioning of the core grid. The library can be downloaded at:

<http://www.netlib.org/scalapack/>

It relies on the BLACS framework, which is available at

<http://www.netlib.org/blacs>

To compile the code with the Scalapack library, switch `USE_SCALAPACK` to 1 in the project Makefile. Note that Scalapack requires a multi-core grid and can therefore not be used in serial mode: it requires to set `USE_MPI` to 1 in the Makefile. Optimal performance can be obtained by also allowing multi-threading. The syntax of the command line is unchanged compared to the basic MPI or hybrid model. However, special care must be taken in the choice of the number of cores: the total number of cores is now the product of the number of cores for each HFB calculation (size of the Scalapack process grid) by the number of different HFB calculations required (defined in `hfodd_mpiio.d`).

## 6 Acknowledgments

We thank Michał Opala for performing OpenMP tests and bringing our attention to Amdahl's law. Discussions with Hai Ah Nam on scaling properties on leadership class computers are also warmly acknowledged. This work was supported in part by the Polish Ministry of Science and Higher Education under Contract Nos. N N202 328234 and N N202 231137, by the Academy of Finland and University of Jyväskylä within the FIDIPRO program, by the UNEDF SciDAC Collaboration under the U.S. Department of Energy grants No. DE-FC02-07ER41457 and DE-FG02-96ER40963 (University of Tennessee), and was partly performed under the auspices of the US Department of Energy by the Lawrence Livermore National Laboratory under Contract DE-AC52-07NA27344 (code release number: LLNL-CODE-470611, d ../.document release number: LLNL-JRNL-472093). Funding was also provided by the United States Department of Energy Office of Science, Nuclear Physics Program pursuant to Contract DE-AC52-07NA27344 Clause B-9999, Clause H-9999 and the American Recovery and Reinvestment Act, Pub. L. 111-5. Computational resources were provided in part by a computational grant from the Interdisciplinary Centre for Mathematical and Computational Modeling (ICM) of the Warsaw University, by the Oak Ridge Leadership Computing Facility, located in the National Center for Computational Sciences at Oak Ridge National Laboratory supported by the Office of Science of the U.S. Department of Energy under Contract DE-AC05-00OR22725, as well as by the National Energy Research Scientific Computing Center supported by the Office of Science of the U.S. Department of Energy under Contract No. DE-AC02-05CH11231. We also acknowledge the CSC - IT Center for Science Ltd, Finland for the allocation of computational resources.

# A Test Run Input

```
!-----!
! This file is part of the official HFODD v2.49t release and demonstrates !
! the use of isospin mixing and projection. !
!-----!
```

```

----- General data -----
NUCLIDE      IN_FIX  IZ_FIX
              20    20
ITERATIONS   NOITER
              100
ITERAT_EPS   EPSITE
              0.000000001
SLOW_DOWN    SLOWEV  SLOWOD
              0.5    0.5
PRINT_ITER   IPRSTA  IPRMID  IPRSTO
              0      0      1
MAXANTIOSC   NULAST
              3
BROYDEN      IBROYD  N_ITER  ALPHAM  BROTRI
              1      7      0.3  10000.0

----- Interaction -----
SKYRME-SET   SKYRME
              SV
SKYRME-STD   ISTDAND  KETA_J  KETA_W  KETACM  KETA_M
              0      1      0      0      1
LANDAU       LANODD  XO_LAN  X1_LAN  GO_LAN  GOPLAN  G1_LAN  G1PLAN
              000    1.0    1.0    0.4    1.2    -0.19  0.62
EVE_SCA_TS   RHO      RHOD    LPR     TAU     SCU     DIV
              1.  1.  1.  1.  1.  1.  1.  1.
ODD_SCA_TS   SPI      SPID    LPS     CUR     KIS     ROT
              1.  1.  1.  1.  1.  1.  1.  1.
EVE_SCA_PM   RHO      RHOD    LPR     TAU     SCU     DIV
              1.  1.  1.  1.  1.  1.  1.  1.
ODD_SCA_PM   SPI      SPID    LPS     CUR     KIS     ROT
              1.  1.  1.  1.  1.  1.  1.  1.

----- Pairing -----
PAIRING      IPAIRI
              0
HFB          IPAHFB
              0
```

```

----- Symmetries -----
ROTATION      IROTAT
              1
SIMPLEXY      ISIMPY
              0
SIGNATUREY    ISIGNY
              0
PARITY        IPARTY
              0
TSIMPLEX3D    ISIMTX  ISIMTY  ISIMTZ
              0      0      0

```

```

----- Configurations -----
PHNONE_NEU    PARTICLES    HOLES
              1            000      000
PHNONE_PRO    PARTICLES    HOLES
              1            000      000
DIANON_NEU
              24  23  0
DIANON_PRO
              24  23  0
VACSIM_NEU    SIMP  SIMM
              12  12
VACSIM_PRO    SIMP  SIMM
              10  10
VACPAR_NEU    PARP  PARM
              14  10
VACPAR_PRO    PARP  PARM
              14   6

```

```

---- Parameters of the HO basis ----
BASIS_SIZE    NOSCIL  NLIMIT  ENECUT
              10     286    800.0
SURFAC_PAR    INNUMB  IZNUMB  ROPARM
              20     20     1.23
OPTI-GAUSS    IOPTGS
              1
GAUSHERMIT    NXHERM  NYHERM  NZHERM
              26     26     26
SURFAC_DEF    LAMBDA  MIU     ALPHAR
              -2     0      0.0
              4     0      0.0

```

```

----- Constraints -----
OMEGAY        OMEGAY

```

```

      0.00
OMEGA_XYZ  OMEHAX  OMEHAY  OMEHAZ  ITILAX
            0.000  0.000  0.000  0
MULTCONSTR LAMBDA   MIU    STIFFQ  QASKED  IFLAGQ
            -2    0     0.25  0.200  1
            2    2     0.25  0.000  1

            ----- Output-file parameters -----
EALLMINMAX EMINAL  EMAXAL
            -30.0  10.0

            ----- Files -----
REVIEWFILE  FILREV
             ca40_iso.rev
RECORDFILE  FILREC
             ca40_iso.rec
REPLAYFILE  FILREP
             ca40_iso.rec
REC_FIELDS  FILFIC
             ca40_iso.fil
REP_FIELDS  FILFIP
             ca40_iso.fil
COULOMFILE  FILCOU
             ca40_iso.cou
REVIEW      IREVIE
             0
RECORDSAVE  IWRIRE
             1
COULOMSAVE  ICOULI  ICOULO
             1      1
FIELD_SAVE  IWRIFI
             1
FIELD_OLD   IWRIOL
             1

            ----- Starting the iteration -----
RESTART     ICONTI
             0
CONTFIELDS  IFCONT
             0
CONT_PAIRI  IPCONT
             0

            ----- Calculate -----
EXECUTE

```

```

----- Next run -----
ITERATIONS  NOITER
             30
SLOW_DOWN   SLOWEV  SLOWOD
             0.5    0.5
BROYDEN     IBROYD  N_DUMM  ALPHAM  BROTRI
             0      7      0.3    10000.0
MULTCONSTR  LAMBDA  MIU     STIFFQ  QASKED  IFLAGQ
             -2     0      0.25   0.200   0
             2     2      0.25   0.000   0
COULOMBPAR  ICOTYP  ICOUDI  ICOUEX
             5      2      2
RESTART     ICONTI
             1
CONTFIELDS  IFCONT
             1
CONT_PAIRI  IPCONT
             0

```

```

----- Calculate -----
EXECUTE

```

```

----- Next run -----
ITERATIONS  NOITER
             1
SLOW_DOWN   SLOWEV  SLOWOD
             1.0    1.0
KERNELFILE  FILKER
             ca40_iso.ker
SAVEKERNEL  ISAKER
             1
PARAKERNEL  IPAKER  NUASTA  NUASTO  NUGSTA  NUGSTO
             0      1      1      1      1
PROJECTGCM  IPRGCM  IPROMI  IPROMA  NUAKNO  NUBKNO  KPROJE  IFRWAV  ITOWAV  IWRWAV
             1      0      0      1      1      0      1      1      0
CUTOVERLAP  ICUTOV  CUTOVE  CUTOVF
             1      1.0E-05  1.0
PROJECTISO  IPRGCM  ISOSAD  NBTKN0  EPSISO  ICSKIP  IFERME
             1      10     8      1.D-10  0      0
RESTART     ICONTI
             1
CONTFIELDS  IFCONT
             1
CONT_PAIRI  IPCONT
             0

```

----- Calculate -----  
EXECUTE  
----- Terminate -----  
ALL\_DONE

## B Test Run Output

```
*****  
*                                                                 *  
*           S I N G L E - C O R E   V E R S I O N           *  
*                                                                 *  
*****  
*           HFODD   HFODD   HFODD   HFODD   HFODD   HFODD   HFODD   HFODD   *  
*                                                                 *  
*****  
*           SKYRME-HARTREE-FOCK-BOGOLYUBOV CODE VERSION: 2.49T *  
*                                                                 *  
*           NO SYMMETRY-PLANES AND NO TIME-REVERSAL SYMMETRY *  
*                                                                 *  
*           DEFORMED CARTESIAN HARMONIC-OSCILLATOR BASIS *  
*                                                                 *  
*****  
*                                                                 *  
*           J. DOBACZEWSKI, B.G. CARLSSON, J. DUDEK, J. ENGEL *  
*           J. MCDONNELL, P. OLBRATOWSKI, P. POWALOWSKI, M. SADZIAK *  
*           J. SARICH, W. SATULA, N. SCHUNCK, J.A. SHEIKH *  
*           A. STASZCZAK, M. STOITSOV, P. TOIVANEN, M. ZALEWSKI *  
*           AND H. ZDUNCZUK *  
*                                                                 *  
*           INSTYTUT FIZYKI TEORETYCZNEJ, WARSZAWA *  
*           LAWRENCE LIVERMORE NATIONAL LABORATORY, USA *  
*                                                                 *  
*           1993-2011 *  
*                                                                 *  
*****  
*                                                                 *  
*           CODE COMPILED WITH THE FOLLOWING ARRAY DIMENSIONS AND SWITCHES: *  
*                                                                 *  
*****
```

```

*
* NDBASE = 680 NDSTAT = 680 NDXHRM = 40 NDYHRM = 40 NDZHRM = 40 *
*
* NDMAIN = 16 NDMULT = 9 NDMULR = 4 NDLAMB = 9 NDITER = 5000 *
*
* NDAKNO = 1 NDBKNO = 1 NDPROI = 20 NDCOUL = 80 NDPOLS = 25 *
*
* NDPROT = 10 NDBTKN = 10 *
*
* IPARAL = 0 I_CRAY = 0 *
*
*
* PRE-PROCESSOR OPTIONS: *
*
*      switch_port = 1      switch_diag = 3      switch_cray = 0 *
*
*      switch_nagl = 0      switch_quad = 0      switch_vect = 1 *
*
*****
:
*****
*
* BROYDEN METHOD IS: ON *
*
* TRIGGERED ONLY WHEN STABILITY IS LOWER THAN : 10000.000 MEV *
* INITIAL SLOWING FACTOR (BEFORE TRIGGER) : 0.50 (=SLOWEV) *
* BROYDEN SLOWING FACTOR (AFTER TRIGGER) : 0.70 (=1-ALPHAM) *
* NUMBER OF ITERATIONS RETAINED IN MEMORY : 7 *
*
*****
:
*****
*
* ONLY THE ISOSPIN PROJECTION IS PERFORMED *
* 8 GAUSS-LEGENDRE KNOTS IS USED *
*
*****
:
*****
*

```

```

*      CUT-OFF "EPSISO" = 0.00000000010000 ==> GOOD-T BASIS OF DIM = 4      *
*                                                                              *
*****
*                                                                              *
*              ISOSPIN-MIXED EIGENSTATES                                     *
*              -----                                                         *
*                                                                              *
*      N      EIGENENERGY      i      T      |C_i|^2      Re[C_i]      Im[C_i]      *
*                                                                              *
*      1      -342.860677      1      0      0.994703      0.997348      0.000000      *
*                                                                              *
*                                                                              *
*                                                                              *
*                                                                              *
*                                                                              *
*      2      -300.253660      1      0      0.005276      0.072636      0.000000      *
*                                                                              *
*                                                                              *
*                                                                              *
*                                                                              *
*      3      -258.016938      1      0      0.000021      -0.004628      0.000000      *
*                                                                              *
*                                                                              *
*                                                                              *
*      4      -215.384252      1      0      0.000000      0.000241      0.000000      *
*                                                                              *
*                                                                              *
*                                                                              *
*      1      -342.860677      2      1      0.005296      0.072772      0.000000      *
*                                                                              *
*      3      2      0.000002      0.001316      0.000000      *
*      4      3      0.000000      -0.000061      0.000000      *
* DOMINANT AMPLITUDE SQUARED EQUALS: 0.9947025220 AND CORRESPONDS TO T = 0      *
* COULOMB MIXING IN THIS STATE IS: 0.0052974780 [ 0.529748%]                  *
*                                                                              *
*                                                                              *
*      2      -300.253660      2      1      0.988062      -0.994013      0.000000      *
*                                                                              *
*      3      2      0.006659      -0.081605      0.000000      *
*      4      3      0.000003      -0.001655      0.000000      *
* DOMINANT AMPLITUDE SQUARED EQUALS: 0.9880618341 AND CORRESPONDS TO T = 1      *
* COULOMB MIXING IN THIS STATE IS: 0.0119381659 [ 1.193817%]                  *
*                                                                              *
*                                                                              *
*      3      -258.016938      2      1      0.006609      0.081296      0.000000      *
*                                                                              *
*      3      2      0.985082      -0.992513      0.000000      *
*      4      3      0.008288      -0.091039      0.000000      *
* DOMINANT AMPLITUDE SQUARED EQUALS: 0.9850815887 AND CORRESPONDS TO T = 2      *
* COULOMB MIXING IN THIS STATE IS: 0.0149184113 [ 1.491841%]                  *
*                                                                              *
*                                                                              *
*      4      -215.384252      2      1      0.000033      -0.005784      0.000000      *
*                                                                              *
*      3      2      0.008257      0.090869      0.000000      *
*      4      3      0.991709      -0.995846      0.000000      *
* DOMINANT AMPLITUDE SQUARED EQUALS: 0.9917092280 AND CORRESPONDS TO T = 3      *
* COULOMB MIXING IN THIS STATE IS: 0.0082907720 [ 0.829077%]                  *
*                                                                              *
*                                                                              *
*****

```

## References

- [1] J. Dobaczewski and J. Dudek, *Comput. Phys. Commun.* **102**, 166 (1997).
- [2] J. Dobaczewski and J. Dudek, *Comput. Phys. Commun.* **102**, 183 (1997).
- [3] J. Dobaczewski and J. Dudek, *Comput. Phys. Commun.* **131**, 164 (2000).
- [4] J. Dobaczewski and P. Olbratowski, *Comput. Phys. Commun.* **158**, 158 (2004).
- [5] J. Dobaczewski and P. Olbratowski, *Comput. Phys. Commun.* **167**, 214 (2005).
- [6] J. Dobaczewski, W. Satuła, B.G. Carlsson, J. Engel, P. Olbratowski, P. Powałowski, M. Sadziak, J. Sarich, N. Schunck, A. Staszczak, M.V. Stoitsov, M. Zalewski, and H. Zduniczuk, *Comput. Phys. Commun.* **180**, 2361 (2009).
- [7] J. Dobaczewski, W. Satuła, B.G. Carlsson, J. Engel, P. Olbratowski, P. Powałowski, M. Sadziak, J. Sarich, N. Schunck, A. Staszczak, M.V. Stoitsov, M. Zalewski, and H. Zduniczuk, *HFODD (v2.40h) User's Guide: arXiv:0909.3626* (2009).
- [8] W. Heisenberg, *Z. Phys.* **77**, 1 (1932).
- [9] E.P. Wigner, *Phys. Rev.* **51**, 106 (1937).
- [10] C.A. Engelbrecht and R.H. Lemmer, *Phys. Rev. Lett.* **24**, 607 (1970).
- [11] E. Caurier, A. Poves, and A. Zucker, *Phys. Lett. B* **96**, 11 (1980); **96**, 15 (1980).
- [12] M. Rafalski, W. Satuła, and J. Dobaczewski, *Int. J. Mod. Phys. E***18**, 958 (2009).
- [13] W. Satuła, J. Dobaczewski, W. Nazarewicz, and M. Rafalski, *Phys. Rev. Lett.* **103**, 012502 (2009).
- [14] W. Satuła, J. Dobaczewski, W. Nazarewicz, and M. Rafalski, *Phys. Rev. C* **81**, 054310 (2010).
- [15] W. Satuła, J. Dobaczewski, W. Nazarewicz, and M. Rafalski, submitted to *Acta Physica Polonica* (2010); arXiv:1010.3099.
- [16] W. Satuła, J. Dobaczewski, W. Nazarewicz, M. Borucki, and M. Rafalski, submitted to *Int. J. Mod. Phys.* (2010); arXiv:1010.5053 .
- [17] W. Satuła, J. Dobaczewski, W. Nazarewicz, and M. Rafalski, submitted to *Phys. Rev. Lett.* (2011); arXiv:1101.0139.
- [18] D.A. Varshalovich, A.N. Moskalev, and V.K. Khersonskii, *Quantum Theory of Angular Momentum* (World Scientific, Singapore, 1988).
- [19] M. Anguiano, J.L. Egido, and L.M. Robledo, *Nucl. Phys.* **A696**, 467 (2001).
- [20] L.M. Robledo, *Int. J. Mod. Phys. E* **16**, 337 (2007).

- [21] J. Dobaczewski, M.V. Stoitsov, W. Nazarewicz, and P.-G. Reinhard, Phys. Rev. C **76**, 054315 (2007).
- [22] H. Zduńczuk, J. Dobaczewski, and W. Satuła, Int. J. Mod. Phys. E **16**, 377 (2007).
- [23] I.S. Towner and J.C. Hardy, Phys. Rev. C **77**, 025501 (2008).
- [24] H. Zduńczuk, W. Satuła, J. Dobaczewski, and M. Kosmulski, Phys. Rev. C **76**, 044304 (2007).
- [25] A.L. Goodman, Nucl. Phys. A **352**, 45 (1981).
- [26] M. Diebel, K. Albrecht and R.W. Hasse, Nucl. Phys. A **355**, 66 (1981).
- [27] P. Bonche, S. Levit and D. Vautherin, Nucl. Phys. A **436**, 265 (1985); **427**, 278(1984).
- [28] J.L. Egido, L.M. Robledo and V. Martin, Phys. Rev. Lett. **85**, 26 (2000).
- [29] V. Martin, J.L. Egido and L.M. Robledo, Phys. Rev. C **68**, 034327(2003).
- [30] J. Dobaczewski, H. Flocard and J. Treiner, Nucl. Phys. A **422**, 103 (1984).
- [31] J.C. Pei, W. Nazarewicz, J. A. Sheikh and A. K. Kerman, Phys. Rev. Lett. **102**, 192501 (2009).
- [32] J.A. Sheikh, W. Nazarewicz and J.C. Pei, Phys. Rev. C **80**, 011302(R) (2009).
- [33] H.J. Lipkin, Ann. of Phys., **9**, 272 (1960).
- [34] J. Dobaczewski, J. Phys. G: Nucl. Part. Phys. **36**, 105105 (2009).
- [35] P. Ring and P. Schuck, *The Nuclear Many-Body Problem* (Springer-Verlag, Berlin, 1980).
- [36] V.M. Strutinsky, Nucl. Phys. A **95**, 420 (1967).
- [37] V.M. Strutinsky, Nucl. Phys. A **122**, 1 (1968).
- [38] M.J. Giannoni and P. Quentin, Phys. Rev. C **21**, 2060 (1980); Phys. Rev. C **21**, 2076 (1980).
- [39] M. Bolsterli, E.O. Fiset, J.R. Nix, and J.L. Norton, Phys. Rev. **C5**, (1972) 1050.
- [40] T.R. Werner and J. Dudek, Atomic Data and Nucl. Data Tables **50** (1992) 179; AIP Conference Proceedings **259**, ed. by J. Dudek and B. Haas, (American Institute of Physics, New York, 1992), p. 683.
- [41] A.T. Kruppa, M. Bender, W. Nazarewicz, P.-G. Reinhard, T. Vertse, and S. Ówiok, Phys. Rev. C **61**, 034313 (2000).
- [42] T. Vertse, A.T. Kruppa, and W. Nazarewicz, Phys. Rev. C **61**, 064317 (2000).
- [43] B. Gall, P. Bonche, J. Dobaczewski, H. Flocard, and P.-H. Heenen, Z. Phys. **A348**, 183 (1994).

- [44] J. Dobaczewski, P. Borecki, W. Nazarewicz, and M.V. Stoitsov, Eur. Phys. J. **A25**,s01, 541 (2005).
- [45] M.R. Hestenes, J. Optim. Theory Appl. **4**, 303 (1969).
- [46] M.J.D. Powell, *Optimization*, ed. R. Fletcher (Academic Press, New-York 1969), p. 283.
- [47] A. Staszczak, M. Stoitsov, A. Baran, and W. Nazarewicz, Eur. Phys. J. A **46**, 85 (2010).
- [48] J. Dechargé and D. Gogny, Phys. Rev. **C21**, 1568 (1980).
- [49] W. Younes and D. Gogny, Phys. Rev. C **80**, 054313 (2009).
- [50] M.V. Stoitsov, J. Dobaczewski, W. Nazarewicz, and P. Ring, Comput. Phys. Commun. **167**, 43 (2005).
- [51] M.V. Stoitsov, W. Nazarewicz, N. Schunck, IJMP E **18** 816 (2009).
- [52] J. Dobaczewski, M. Stoitsov, and W. Nazarewicz, AIP Conference Proceedings **726**, 52 (2004).
- [53] N. Schunck, J. Dobaczewski, J. Moré, J. McDonnell, W. Nazarewicz, J. Sarich and M. V. Stoitsov, Phys. Rev. C **81** 024316 (2010).
- [54] K.T.R. Davies and S.J. Krieger, Can. J. Phys. **69**, 62 (1991).
- [55] A. Baran, A. Bulgac, M. McNeil Forbes, G. Hagen, W. Nazarewicz, N. Schunck, and M.V. Stoitsov, Phys. Rev. C **78**, 014318 (2008).
- [56] A. Staszczak, A. Baran, J. Dobaczewski and W. Nazarewicz, Phys. Rev. C **80**, 014309 (2009).
- [57] E. Chabanat, *Interactions effectives pour des conditions extrêmes d'isospin*, Université Claude Bernard Lyon-1, Thesis 1995, LYCEN T 9501, unpublished.
- [58] E. Chabanat, P. Bonche, P. Haensel, J. Meyer, and R. Schaeffer, Nucl. Phys. A **635**, 231 (1998).
- [59] M. Kortelainen, T. Lesinski, J. Moré, W. Nazarewicz, J. Sarich, N. Schunck, M. V. Stoitsov, and S. Wild, Phys. Rev. C **82**, 024313 (2010).